Targeted delivery of nucleic acids to cancer associated fibroblast using lipid nanoparticles

Master thesis

Research group AOT-ET

Graduation Committee:
Chairman: Prof. Dr. Jai Prakash
External Member: Dr. Julieta Paez

Daily Supervisor: Kunal Pednekar, MSc.

Małgorzata Marta Tasior (S2042835)

Preface

I would like to express my gratitude to Prof. Dr. Jai Prakash for giving me the opportunity to perform my Master Thesis under his supervision in the Targeted Therapeutics group of the Advanced Organ bioengineering and Therapeutics department as well as being the chair for my final graduation committee. I would like to thank prof. dr. Jai Prakash for his support and his assistance during my assignment

Furthermore, I would like to thank Dr. Julieta Paez for taking the position as the external member of my graduation committee.

Moreover, a special thanks to Kunal Pednekar for supervising me on a daily basis and teaching me the techniques necessary to perform my Master thesis, giving me advice on how to structure my experiments and reviewing the final manuscript.

Abstract

Tumor microenvironment is very complex structure made our extracellular matrix and variety of cells. One of the more prominent cell types are cancer associated fibroblast (CAFs). They are involved in variety of processes that promote tumor growth and development. For years tumors have been treated with traditional therapies such as radiotherapy or chemotherapy. However, they all have their own drawback and lead to reduced quality of life for patients. That is why alternative treatment are gaining more popularity. One of them are nucleic acid therapeutics. However, they also have their own drawbacks like the need to be delivered using a vesicle that will be able to protect them and assist in cell membrane penetration. The purpose of this study was to produce lipid nanoparticles (LNPs) that will be able to encapsulate nucleic acid for targeted delivery to cancer associated fibroblasts. Ionizable lipid Dlin-MC3-DMA (MC3) was used to encapsulate nucleic acids. Various factors were taken into consideration during the LNPs production process. Those include flow rate, lipid:RNA volume ratio and dye usage. Moreover, conjugation and purification were also adjusted to further optimize the process. AV3 molar excess, TCEP usage and purification methods were shown to impact the size of the LNPs. All tested conditions resulted in lipid nanoparticles capable of nucleic acid encapsulation. To proceed with in vitro studies, pancreatic stele cells (PSCs) treated with transforming growth factor beta (TGF-β) were tested to see if they were activated and had overexpressed integrin alpha-5 (ITGα5). qPCR proved activation of PSCs with TGF-β. Additionally immunostaining and qPCR proved overexpression of ITGα5 on treated cells. Uptake studies confirmed that AV3 conjugated LNPs are capable of targeting activated PSCs. Transfection studies demonstrated targeting and nucleic acid delivery by LNPs-AV3.

Summary

Cancer is one of the most common and deadly disease in the world. In 2020 alone there were over 19 million new cases and nearly ten million deaths caused by this disease. [1] In the past it was believed that tumors are solely made out of cancer cells. However, it was proven that tumor mass is made out of extracellular matrix (ECM) and variety of cells apart from cancer cells, such as tumor associated macrophages, B cells, T cells, NK cells, cancer associated fibroblasts etc. Cancer associated fibroblasts are a very attractive target due to their involvement in variety of pro-tumorigenic processes in tumor microenvironment (TME). In a study done by Kuninty et al. [2] it was shown that ITGα5 is overexpressed on PSCs activated with TGF-β, which in quiescent state are precursors for CAFs in pancreas.

When it comes to cancer treatment there are several traditional therapies such as radiotherapy, chemotherapy or surgical removal. However each of the available treatments has its own downsides that decrease patient's quality of life with various degrees of success reaching the therapeutic goal. That is why more and more research is being done looking for alternative therapies. Nucleic acid therapeutics are one of them. They are nucleic acids that can be used for gene therapy, RNA expression or DNA inhibition.[3] While they do have desirable qualities, they also have a few disadvantages including negative charge that prevents them from penetrating cell membrane and they are susceptible to nucleases.[4] That is why they need a vessel that will be able to deliver them safely to their target. One of such a criers are lipid nanoparticles. They have plenty of advantages such as biocompatibility and ability to adjust their properties by changing their components. In order to encapsulate the nucleic acids inside LNPs ionizable lipids are employed, more specifically Dlin-MC3-DMA. Their ability to become protonated at lowered pH allows for easy encapsulation during fabrication process and facilitates endosomal escape inside the cell.

In this study, in order to produce lipid nanoparticles we used microfluidic device that allowed to create optimal LNP assembly conditions by applying chaotic mixing during fabrication. Fabrication and conjugation process were optimized to produce LNPs with acceptable characteristics. Different factors were taken into consideration such as flow rate, lipid:RNA ratio, purification etc. Nanoparticles were able to encapsulate the nucleic acids. To confirm that activated PSC can be targeted by LNPs-AV3, cells treated with TGF-β and quiescent cells were tested using immunostaining and qPCR. In vitro studies done on PSCs included uptake and transfection studies. LNPs-sAV3 were used as a control in both, uptake and transfection studies. Unconjugated LNPs were used as an additional control in transfection experiments. The studies showed that LNPs-AV3 were able to target activated PSCs and deliver nucleic acid to them.

All in all, this research was able to produce LNPs that encapsulate nucleic acid and were able to target activated PSCs. Moreover they are also able to deliver nucleic acid to targeted cells. This research gives basis for further development of nucleic acid delivery platform to activated fibroblast.

Table of content

1. Introduction

1.1. Cancer

For years cancer has been one of the most prominent disease in the world. In 2022 it was estimated by GLOBOCAN that there were 19,292,789 new cancer diagnosis and 9,958,133 cancer related death. Europe share of total cancer cases was 22.8%, while it accounted for 19.6% of deaths. It is significant statistic as Europe makes up only 9.7% of world population [5] It is important to note that diagnosis and treatment in 2020 were often delayed due to the coronavirus disease and it is not yet determined what the long term effects will be. [6] Pancreatic cancer is one of the most diagnosed cancer with 7.3% of all new cases in a year. It is also one of the leading mortality cause for men. [5] However, that does not mean that pancreatic cancer is not a serious threat to women as well, being the third leading cause of death regardless of gender in USA. It is also predicted to become the third leading cause of death in EU in a next few years.[6][7] In general early detection and improved treatments decreased overall mortalities related to cancer. Nonetheless, that is not the case for pancreatic cancer where instead of decreasing mortality stayed similar for women and it slowly increase for man in years 2000-2019.[6]

Estimated New Cases

Males				Females		
Prostate	268,490	27%		Breast	287,850	31%
Lung & bronchus	117,910	12%		Lung & bronchus	118,830	13%
Colon & rectum	80,690	8%		Colon & rectum	70,340	8%
Urinary bladder	61,700	6%		Uterine corpus	65,950	7%
Melanoma of the skin	57,180	6%		Melanoma of the skin	42,600	5%
Kidney & renal pelvis	50,290	5%		Non-Hodgkin lymphoma	36,350	4%
Non-Hodgkin lymphoma	44,120	4%		Thyroid	31,940	3%
Oral cavity & pharynx	38,700	4%		Pancreas	29,240	3%
Leukemia	35,810	4%		Kidney & renal pelvis	28,710	3%
Pancreas	32,970	3%		Leukemia	24,840	3%
All Sites	**983,160**	**100%**		**All Sites**	**934,870**	**100%**

Estimated Deaths

Males				Females		
Lung & bronchus	68,820	21%		Lung & bronchus	61,360	21%
Prostate	34,500	11%		Breast	43,250	15%
Colon & rectum	28,400	9%		Colon & rectum	24,180	8%
Pancreas	25,970	8%		Pancreas	23,860	8%
Liver & intrahepatic bile duct	20,420	6%		Ovary	12,810	4%
Leukemia	14,020	4%		Uterine corpus	12,550	4%
Esophagus	13,250	4%		Liver & intrahepatic bile duct	10,100	4%
Urinary bladder	12,120	4%		Leukemia	9,980	3%
Non-Hodgkin lymphoma	11,700	4%		Non-Hodgkin lymphoma	8,550	3%
Brain & other nervous system	10,710	3%		Brain & other nervous system	7,570	3%
All Sites	**322,090**	**100%**		**All Sites**	**287,270**	**100%**

Figure 1. Ten leading cancer types with estimated new cancer cases and estimated deaths by sex, United States, 2022. Estimates are rounded to nearest 10. Rankings based on modeled projections and may differ from recent data [6]

Word cancer refers to a class of diseases that possess abnormal cell growth and tissue penetration. There are several key capabilities that are connected with cancer. They are: sustaining proliferative signaling, evading growth suppressors, activating invasion and metastasis, enabling replicative immortality, inducing angiogenesis and resisting cell death. [8] However, it is important to remember that each cancer is different and might have different composition, causes and is susceptible to different treatments.[9] That is why it is important to know what type is under consideration in order to find the most efficient treatment options.

1.2. Tumor microenvironment

For decades it was believed that tumor are solely made out of cancer cells. The discovery that apart from cancer cells other components are involved in creating tumor, it change the way that this disease is being approached today. Tumor microenvironment is structure made out of variety of components. They are generally divided into extracellular matrix and cellular components (Figure 2). Extracellular matrix (ECM) is a non-cellular component of TME. Depending on tumor types ECM can be made of various components. Some of them include fibronectin, elastin, laminins and fibrillary collagen.[10] It provides structural support to the cellular components and reservoir of growth factors and cytokines. However, it is not just a scaffold for cells or a storage place, ECM is an active contributor of TME by partaking in cell adhesion, facilitates cell-cell interactions and cell proliferation. [11][12] Degradation of ECM creates bioactive fragments that are utilized in various events such as tissue remodeling, angiogenesis, metastasis, tumor growth, and inflammation. [12][13][14]

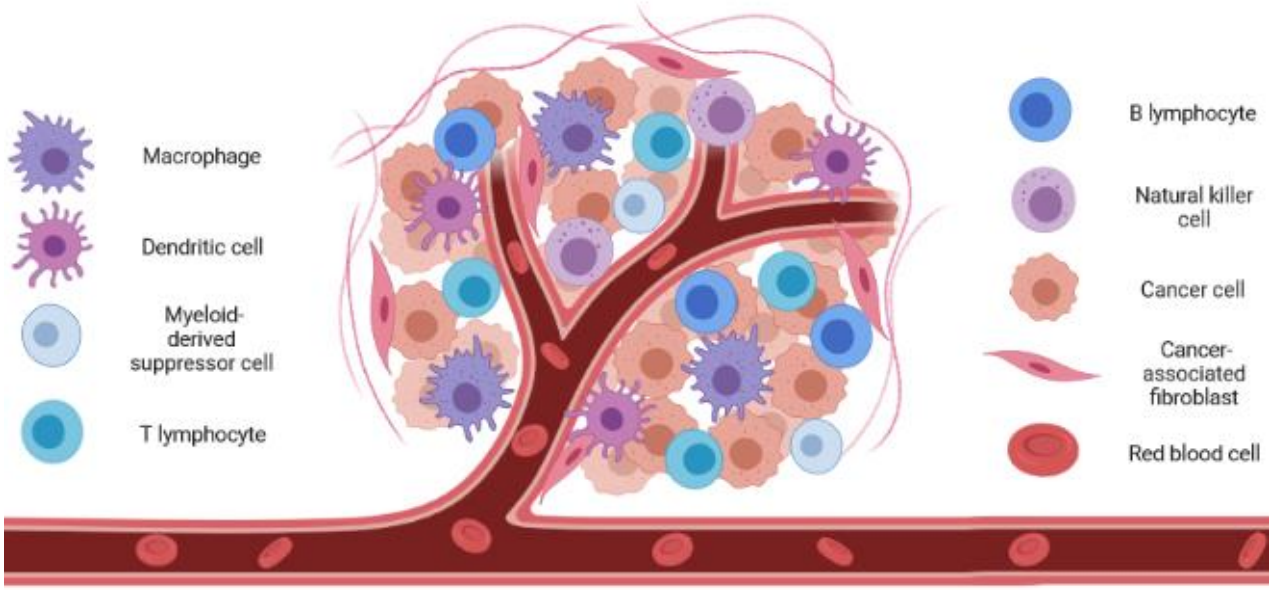

Figure 2. Schematic representation of the tumor microenvironment (TME) including extracellular matrix (ECM) and different nonmalignant cellular components. Created with Biorender.com

Apart from ECM tumor possess variety of cellular components. Their composition varies depending on a tumor type. Some of the cellular components include tumor associated macrophages (TAMs), cancer associated fibroblast (CAFs), T lymphocytes, B lymphocytes, natural killer (NK) cells, cancer cells etc. Each of the components have its own tasks, but it also interacts with other cells in the TME.

When it comes to T cells, there are cells like cytotoxic CD8+ memory T cells which have the ability to kill cancer cells [15], but there are also tumor promoting cells such as $CD4^{+}$T cells or the immunosuppressive T regulatory cells (Tregs). Tregs prevent the immune system from inhibiting recognition and clearance of tumor cells. [16] B cells are responsible for cytokines secretion, production of antibodies and antigen presentation. Usually, they are found on the tumors margins, very few penetrate TME to go deeper. Depending on cancer type they can have pro-tumorigenic or anti-tumorigenic effect when found inside TME. [17] NK cells are not always found in TME, but when they are they usually indicate better prognosis. Cells can be divided into cells that secrete cytokines that facilitate immune response and cancer cells killers.[18] Dendritic cells are responsible for antigen processing and presentation. [19] They are programed to have anti-tumorigenic function. However, due to the cytokines in TME they can be triggered to tolerate the environment and support tumor progression. [17] Tumor associated macrophages (TAM) are one of the more commonly present cells in TME. Macrophages are the immune cells that are responsible for pathogen phagocytosis and presentation of antigen. TAMs can have various types of polarization. However, they are usually categorized as M1- and M2-polarized macrophages. M1-polarized macrophages are inflammatory macrophages and usually phagocytize and kill cells. M2-polarized macrophages are anti-inflammatory i.e. immune-suppressive. They are the ones that are usually pro-tumorigenic. Both types can be present in TME. However, due to different cytokines and hypoxia present in TME usually M2-polarized macrophages are more abundant as they support tumor growth and proliferation. [17][20][21][22] These are just some examples of cells that can facilitate pro-tumorigenic conditions. That shows that tumor microenvironment is very complex structure with many components that can interact with each other. The cells that this study focuses on are cancer associated fibroblast discussed below.

1.3. Cancer associated fibroblasts and their role in TME

Cancer associated fibroblast are highly heterogeneous population of cells that can be found in TME. Often they make up large part of TME. CAFs can originate from variety of cells including stellate cells, adipocytes, mesenchymal stem cells , resident fibroblasts, bone marrow-derived MSCs, epithelial cells, endothelial cells, hematopoietic stem cells pericytes and fibrocytes. They are each activated by different factors. The only factor that works on all types of cells is transforming growth factor beta (TGF-β). [23][24] CAFs are involved in variety of pro-tumoigenic functions such as cancer cell stemness generation and maintenance, angiogenesis, ECM synthesis and remodeling, immune regulation internal environment stability, metabolic response and therapeutic resistance [24][25][26][27][28][29] CAFs are major sources of chemokines, cytokines, EVs, multiple proteins, ECM, various enzymes and growth factors. [24] They are also highly involved in interactions with other cells in TME (Figure 3). It was shown that they are capable of recruiting macrophages into the TME. [30][31] They also promote M2-polarization among recruited macrophages.[32] CAFs are also involved in recruitment and subsequent differentiation and survival of T cells. That allows for the creation and upkeep of immunosuppressive environment. Moreover, they can affect dendritic cells in such a way that it will result in inhibition of their ability to present antigens as well as the ability that activate cytotoxic T cell responses. [32][33] These are just a few examples of how CAF interactions with other cells in TME affect pro-tumorigenic process. In recent years it has been shown that there are various subtypes of CAFs that can be found in TME. They include myofibroblastic CAF (myCAF), inflammatory CAF (iCAF) and antigen-presenting CAFs (apCAFs). [34][35] All of them impact tumor microenvironment in different ways. As we can

see CAFs are involved in variety of pro-tumorigenic processes in TME that is what makes them such an interesting target for delivering therapeutics.

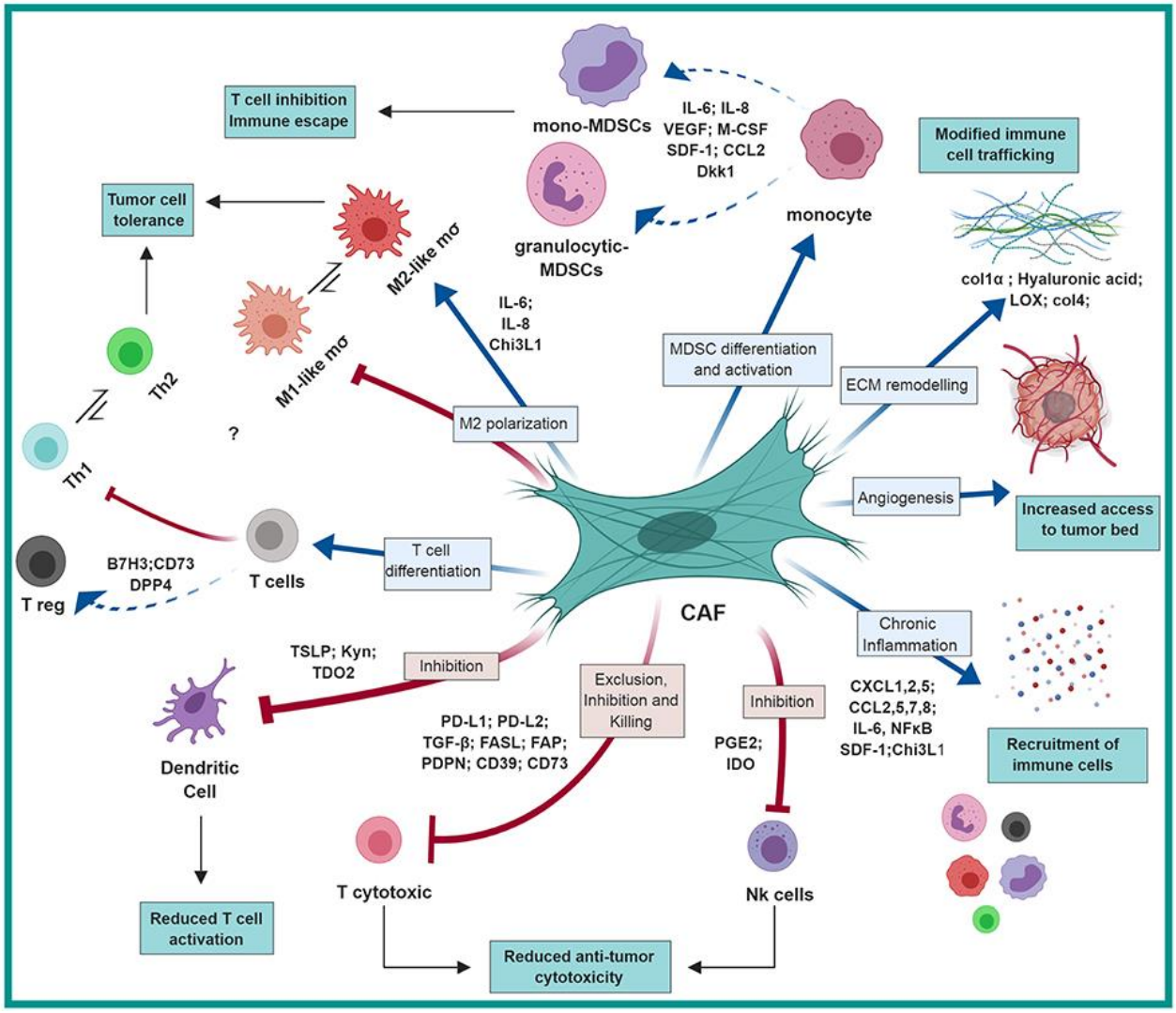

Figure 3. CAF interactions with other components of TME.[32]

1.4. CAF targeting

CAFs due to their versatility in variety of processes are attractive target for targeted therapeutics. In a study done by Kuninty et al. [2] they showed that ITGα5 is overexpressed on pancreatic stellate cells (PSCs). In case of pancreatic cancer PSCs are cells from which CAFs originate. Normally quiescent PSCs are present in small amounts. However, during tumorigenic processes they become activated and transition to myofibroblasts that are detectable by upregulation of α-smooth muscle actin (α-SMA). In this study they developed novel short peptidomimetic (AV3) that is able to target ITGα5. AV3 structure is presented on Figure 4a. AV3 can be adjusted to enable its conjugation to desired carrier. There are various ways in which AV3 can be conjugated to a carrier. One of possible modifications is addition of

thiol group. Thiol group can undergo a click chemistry reaction with maleimide (Figure 4b) and connect two substances together, creating a vesicle that can target activated PSC.

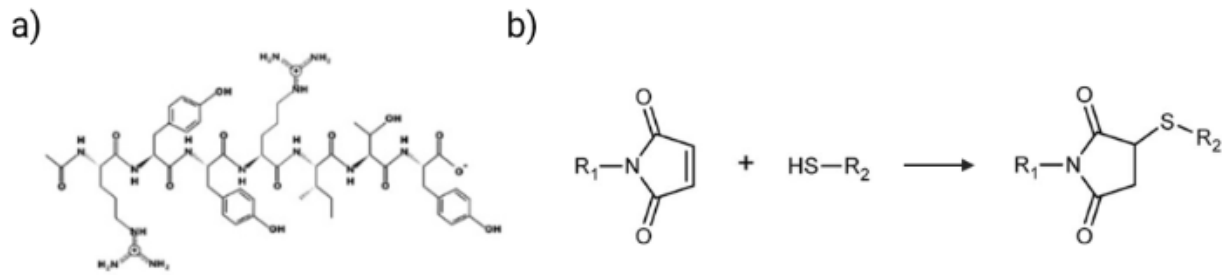

Figure 4. a) AV3 structure[2] b) Click reaction of thiol and maleimide[36]

1.5. Cancer Therapies

There are various ways in which cancer treatment can be approached. Patients can undergo chemotherapy, radiation, surgical intervention, immunotherapy and bone marrow transplant. Ultimately the type of therapies assigned to different patients will vary. The choices are based on variety of factors such as cancer type, cancer stage, age, other underlying medical conditions etc. However, while commercially available therapies can result in successful treatment they still carry a lot of different drawback with them. Some of which include hair loss, diarrhea, nausea, deep vein thrombosis, decreased number of white blood cells, pain and troubles with memory. While it might not sound like a bad tradeoff for, these side effects still bring down patients quality of life. Moreover, in many cases the treatments might not be as effective and might not result in significant health improvement.[37][38] That is why alternative therapies are being investigated more and more, to bring more effective treatments without increasing side effects or treatments that can decrease them.

1.6. Nucleic acid therapeutics

Nucleic acid therapeutics are one of the alternative treatments under development. They are based on usage of nucleic acid for therapeutic purposes. They can be divided into DNA therapeutics and RNA therapeutics (Figure 5). DNA therapeutics include DNA plasmids, viral vectors and CRISPR-Associated Protein 9 (CRISPR-Cas9). DNA plasmids can encode therapeutic proteins. Viral vectors can assist with replacement of missing or defective proteins. At a particular locations in the genome CRISPR-Cas9 is used to add, alter or remove genetic material. RNA therapeutics are mRNA, antisense oligonucleotide (ASO), small interfering RNA (siRNA), aptamers and microRNA. [39] ASOs are small single stranded RNA effective in nucleus, that are able to repress or promote target expression. mRNA encodes a protein. siRNAs are small non-coding, double stranded RNAs that mainly blocks protein translation. miRNAs are small non coding RNAs that have two functions. They can promote targeted mRNA degradation, by binding to the miRNA that was blocking mRNA resulting in free mRNA. On the other hand they can also unlock mRNA translation by binding to a specific corresponding sequence on mRNA. In case of aptamers they are single stranded molecules that created secondary and tertiary structures. Different molecular pathways can be inhibited or promoted due to aptamer interaction with a specific molecule or enzyme[3][39][40][41]

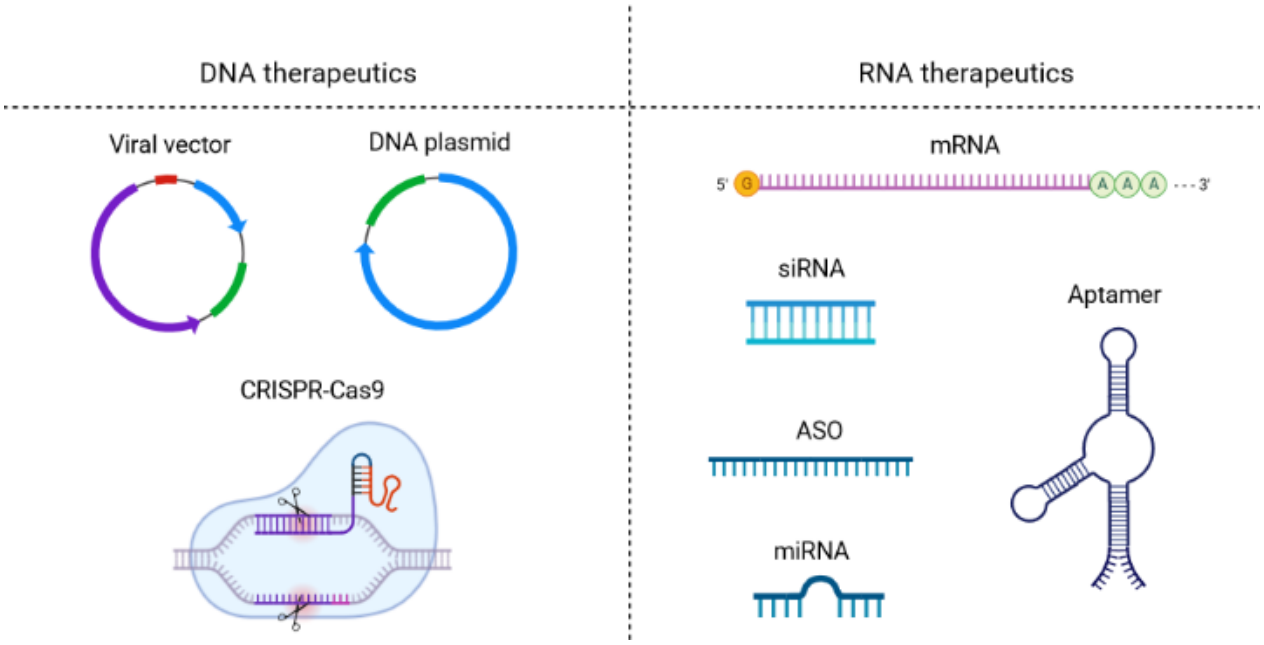

Figure 5. Different kind of nucleic acid therapeutic. Created with Biorender.

Although nucleic acid seam very promising they have their own drawbacks that limit their usage and development. They are also too large to passively pass through a membrane. What is more they are negatively charged due to that they are unable to penetrate cell membrane on their own since cell membranes are negatively charged. Moreover, naked nucleic acids are susceptible to rapid blood clearance, short circulation half-life caused by phagocytosis and to nucleases that can degrade them. Nucleic acids can also cause immune system activation. Apart from that nucleic acid therapeutic are unable to go through with endosomal escape, meaning that they will not be able to reach the cytosol. [42][43][44] That is why they need a vesicle that will be able to transport them to desired place.

1.7. Lipid Nanoparticles

A carrier needs to be used for efficient delivery of nucleic acid therapeutics to their desired destination. There are several options such as micelles, gold nanoparticles, iron oxide nanoparticles polymeric nanoparticles, lipid nanoparticles etc. [41][43] The focus in this paper will be directed to lipid nanoparticles. What makes LNPs such an attractive solution is the fact that they are biocompatible, biodegradable, can carry large payloads and are capable of self-assembly. [45] What is more, it is possible to control their biological characteristics which allows for creation of nanoparticles with wide range of biophysical and physicochemical properties. [46][47][48][49] LNPs are usually made out of helper lipid, cholesterol, PEG-lipid and ionizable lipid. Helper lipids help to create and also destabilize lipid bilayer, which facilitates endosomal escape. Cholesterol assists with structural integrity, LMPs membranes fusion and stability of the formulation. PEG-lipid due to their steric effect barrier can extend circulation time, prevent aggregation or fusion of LNPs. Ionizable lipids help to encapsulate nucleic acid and then assist in their endosomal escape. [50][51][52][53].

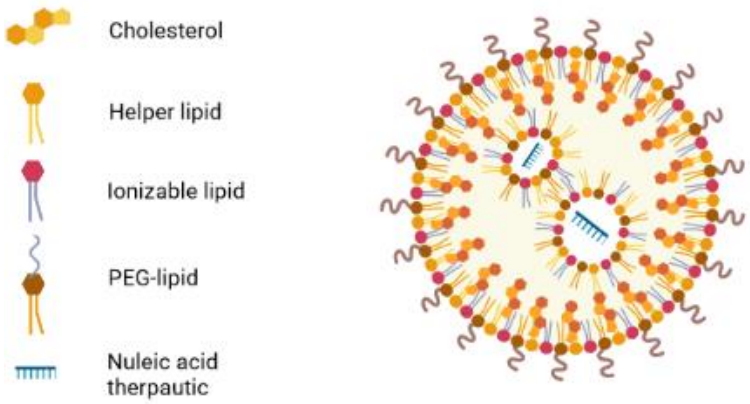

Figure 6.. LNP schematic and building blocks. Created with Biorender.

1.8. Ionizable lipids

Ionizable lipids are created in order to assist in encapsulation of nucleic acid and later on in endosomal escape after LNPs are uptaken by the cells. They are usually composed of three parts: a lipophilic moiety, a linker and an ionizable headgroup. [54] Ionizable lipids become protonated at acidic pH, during that time they can interact with nucleic acid and encapsulate them inside LNPs. When pH is brought back to physiological conditions (pH 7.4) ionizable lipid become neutral again. This is necessary to prevent clearance by other immune cells during circulation, as positively charged nanoparticles are removed by Kaupffer cells or splenic macrophages. After LNPs enter the cell and are inside endosome they should become protonated again due to lower endosomal pH. This change should destabilize endosomal membrane and allow for nucleic acid delivery to cytosol. [55][56] One of the most widely used ionizable lipids is Dlin-MC3-DMA (MC3) (Figure 7). This lipid has been used in variety of studies. [57][58][59] This ionizable lipid has also been used in commercially available medication ONPATTRO[60].

Figure 7.MC3 molecule.

1.9. Goal of the project

In this project lipid nanoparticles that are able to encapsulate and deliver nucleic acids will be prepared. The base of said nanoparticles will be made out of DSPC (helper lipid), cholesterol, PE-PEG. To assist in the encapsulation of nucleic acids ionizable lipid Dlin-MC3-DMA, from now on referred to as MC3, will be used as part of the formulation. Additionally, to enable the attachment of moiety that will be targeting activated fibroblasts, DSPE-PEG-maleimide (DSPE-PEG-MAL) will also be used in the formulation. LNPs with presented components will be made using microfluidic device, that is why formulation condition will have to be adjusted to obtain optimal results. After that LNPs will be conjugated with AV3-Cys-SH, from here on referend to as AV3. Previous research done by the group has shown that AV3 targets ITGα5 that is overexpressed on activated PSC. For satisfactory results the conditions of conjugation and following purification will be adjusted. The particles will be loaded with DiI dye and total RNA of RAW-eGFP positive cells. The only difference will be for LNPs used in transfection studies where, instead of using total RNA of RAW-eGFP positive cells, mix of total RNA RAW-eGFP positive cells:eGFP mRNA (3:1 weight ratio) will be used.

In this study formulations will be characterized using size (nm), polydispersity index (PdI), zeta potential (mV) and encapsulation efficiency (EE). After obtaining LNPs with satisfactory properties they will be tested in vitro. PSC will be used for uptake and transfection studies. To confirm that LNPs conjugated with AV3 will be able to target PSC they will be tested using immunostaining and qPCR. Both test will look for overexpressed ITGα5 on cells activated with TGF-β, while qPCR will look into factors that can confirm that treated PSC are activated fibroblasts. If the results come back positive cells will be used in uptake and transfection studies. DiI signal seen in uptake studies will allow for the identification of LNPs-AV3 targeting and uptake by quiescent and activated PSC, while transfection studies with green GFP signal will be able to assess nucleic acid delivery to cells.

2. Materials and methods

2.1. Chemicals and Materials

Human pancreatic stellate cells (PSCs) were obtained from ScienCell (Carlsbad, CA). Murine RAW 264.7 modified to express eGFP (RAW-eGFP) were kindly gifted to the Advanced Organ bioengineering and Therapeutics - Targeted Therapeutics group, University of Twente. During this study the following lipids were used : 1,2-Distearoyl-sn-glycero-3-phosphocholine (DSPC)(Lipoid, Germany), Cholesterol (Sigma-Aldrich, MO, USA), Lipoid PE 18:0/18:0 PEG-2000 (PE-PEG) (Lipoid, Germany), DSPC-PEG-maleimide (Nanocs ,NY ,USA), D-Lin-MC3-DMA (MC3) (Med-Chem Express, USA). AV3 and sAV3 (China Peptide Co. Ltd., Shanghai, China). mRNA: CleanCap eGFP mRNA (5moU) (Trilink Biotechnologies). Additionally, 1,1′-dioctadecyl-3,3,3′,3′-tetramethylindocarbocyanine) (DiI) dye (Sigma-Aldrich, MO, USA) was used in the LNP preparation. All chemicals used were purchased from Sigma-Aldrich (MO, USA) unless specified otherwise.

2.2. Cell seeding – RAW 264.7 eGFP positive cells

RAW 264.7 eGFP positive cells were cultured in RPMI 1640 medium without L-Glutamine (Lonza Bioscience) supplemented with 10 vol.% Fetal Bovine Serum (FBS), 1 vol% Penicillin/Streptomycin (Pen/Strep) (both from ScienCell) and 1 vol.% L-Glutamine (Thermofisher Scientific) in T75 flask (Cellstar, Greiner bio-one, Kremsmünster, Austria). The cells were maintained at 37ºC in a humidified 5% CO_2 atmosphere and sub-cultured at 80% confluence. Passing and seeding of cells was performed as follows. Cells were washed with warmed Dulbecco's phosphate buffered saline (DPBS) (Lonza, Basel, CH). After that 10 ml of RPMI-1640 medium were added to the T75 flask. Cells were detached with the usage of cell scratcher and transported to a sterile Falcon tube and counted using a hemocytometer (Buerker-Tuerk, Brand GMBH, Wertheim, DE). Passed cells were placed in T25 flask with 1 million cells in 10 ml of medium. For seeding in 24 cell culture well plate (Cellstar, Greiner bio-one, Kremsmünster, Austria), RAW-eGFP positive cells were seeded with 250,000 cells in 500 µl of medium per well. Cells were incubated for 24h at 37ºC in a humidified 5% CO_2 atmosphere. Then they were washed with DPBS two times. Cells without medium were stored at -80ºC for RNA extraction.

2.3. RNA extraction

RNA extraction was used on RAW-eGFP positive cells or PSCs. Extraction was done with the usage of RNA isolation kit (Sigma-Aldrich, MO, USA). Cells were lysed using lysis buffer made out of lysis solution and 1% 2-Mercaploethnaol. Lysate was spinned down using the filtration column at 13.3 RMP for 5 min. The lysate was diluted using 70% ethanol, placed in a binding column and spinned down (13.3 RMP, 1 min). The binding column was washed with wash 1, two times with wash 2 (13.3 RMP, 1 min) and one empty spin (13.3 RMP, 2 min). Elution solution was used to collect RNA form the column (13.3 RMP, 5 min). 2µl of RNA solution were used to determine the RNA concentration using NanoDrop (Nanodrop ND-1000, Wilmington, DE, USA).

2.4. LNP preparation

All surfaces and equipment were cleaned with 0.5 % SDS solution. Lipid stocks were prepared by dissolving lipids in ethanol and were stored at -20ºC. Before usage the lipids were thawed at room temperature. DiI dye was heated up in 70ºC water bath. Lipids were mixed in the following molar ratio 50:10:38.5:1.2:0.3 (DLin-MC3-DMA:DSPC:cholesterol:PEG lipid:PEG lipid with maleimide). Total RNA of RAW-eGFP positive cells was used for the LNP characterization, LNP optimization and uptake studies. For transfection studies, mixture of total RNA from RAW-eGFP positive cells: eGFP mRNA

(3:1 weight ratio) was used. RNA was dissolved in 25 mM of sodium acetate (pH 4.0) to achieve final concentration, after formulation of 10.5 μg/ml. Tested flow rates included 2ml/min, 12 ml/min and 20 ml/min. 1:5 and 1:3 lipid:RNA volume ratios were tested. The formulations were made using microfluidic mixing device Nanoassembler Benchtop (Precisions NanoSystems, BC, Canada). Formulations were dialysed against PBS (pH 7.4) using Slide-A-Liser MINI Dialysis Devices (Thermo Scientific, IL, USA) first for 2h at 4ºC. Then after exchanging PBS the formulation was left to dilyse overnight at 4ºC. LNPs were stored at 4ºC.

2.5. AV3 conjugation

LNPs were conjugated using conjugation mix consisting of AV3 or sAV3, dry Dimethyl sulfoxide (DMSO) and Tris(2-carboxyethyl)phosphine hydrochloride (TCEP) (Thermo-Fisher Scientific, MS, USA). AV3 was added in 3 times molar excess with respect to the amount of DSPC-PEG-Mal used during LNP preparation. TCEP was added in 50 times molar excess with respect to the AV3 used. TCEP was used to avoid the formation of disulfide bonds. Mixed solution was stored under N_2 for 30 min at room temperature. Conjugation mix is slowly added in 1:10 (conjugation mix:LNP) volume ratio to continually vortexed LNP formulation. Created solution was stored at 4ºC overnight and purified the following morning.

2.6. Purification of conjugated LNPs

LNPs were purified in one of 3 ways: dialysis, spin column, desalting column. Slide-A-Liser MINI Dialysis Devices (Thermo Scientific, IL, USA) was used for the dialysis. The LNPs were dialyses for 2h at 4ºC in 155 mM PBS, after that PBS was exchanged and LNPs were left to dialyze at 4ºC overnight. For spin column purification Amicon Ultra-0.5 Centrifugal Filter Unit (Merck Millipore, MA, USA) were used. LNPs were spined down at 4ºC for 15 min at 2000 Rpm. After which they were resuspended in 155 mM PBS to desired volume. PD-10 column (cytiva, Marlborough, USA) was used according to the provided protocol. Column was washed with 155 mM PBS (pH 7.4). and spinned down at the last washing. Sample was loaded on the resin bed and spined down at 1000 G for 2 min. PH was checked using a pH strip. If pH was below 7 then the solution was further dialyzed for 2h at 4ºC to reach 7 pH. LNPs were stored at 4ºC.

2.7. LNPs characterization

LNPs characterization focused on the determination of the size, zeta potential and RNA encapsulation efficiency. Size and zeta potential were measured using Zetasizer Nano ZS (Malvern Instruments, Malvern, UK). For size measurements LNPs formulation was dissolve in 155 mM PBS (pH 7.4) and zeta potential measurements LNP formulation was dissolved in 10 mM KCL. LNPs were dissolved in their respective solvents in a ratio 1:50 to achieve 1 ml of solution containing dissolved LNPs. Encapsulation efficiency was determined using QuantiFluor RNA system (Promega, WI, USA). Provided protocol was adjusted to include broken LNPs so that fluorescence could be measured for unbroken and broken LNPs. In order to break apart the LNPs 2% triton x-100 (Sigma-Aldrich, MO, USA) in 1x TE buffer was used. Fluorescence was measured at 492 nm_{EX}/540 nm_{EM} using Tecan Infinite M200 Pro (Tecan Life Sciences, Männedorf, Switzerland). The encapsulation efficiency was calculated based on the following equation

$$EE = \frac{Amount\ of RNA\ detected\ after\ breaking\ LNPs - Amount\ of\ RNA\ detected\ before\ LNP\ breakage}{Total\ amount\ of\ RNA\ used\ for\ the\ formulation} * 100\%$$

2.8. Cell seeding - PSCs

Pancreatic stellate cells (PSCs) were cultured in Stellate cell medium (SteCell medium) supplemented with 2 vol.% fetal bovine serum (FBS), 1 vol.% stellate cell growth supplement (SteCGS) and 1 vol% penicillin/ streptomycin (Pen/ Strep) (all products from ScienCell). PSC were cultured in T25 flask (Cellstar, Greiner bio-one, Kremsmünster, Austria). The cells were maintained at 37ºC in a humidified 5% CO2 atmosphere and passed at 80% confluence. Passing and seeding of cells was performed as follows. Cells were washed with warmed DPBS. After which they were detached using warmed 500 µl of 1x trypsin/ ethylenediaminetetraacetic acid (EDTA) (Gibco) for 5 min at 37ºC at 5% CO_2. The trypsin/EDTA mix was neutralized by with 4.5 mL SteCell medium and transported to a sterile Falcon tube and spined down for 5 min at 300 G. Medium was replaced and PSC were resuspended in 5ml of warm SteCell medium counted using a hemocytometer (Buerker-Tuerk, Brand GMBH, Wertheim, DE). Passed cells were placed in T25 flask with 200 000 cells in 5 ml of medium. Otherwise cells were seeded in 24 or 96 cell culture well plate (Cellstar, Greiner bio-one, Kremsmünster, Austria). In 96 well plate PSCs were seeded with 2 500 cells in 100 µl of medium per well. For 24 well plate PSCs were seeded with 10 000 cells in 500 µl of medium per well. Cells were incubated for 24h at 37ºC and 5% CO_2. After that the cells were starved with Stellate cell medium (SteCell medium) supplemented with 1 vol.% stellate cell growth supplement (SteCGS) and 1 vol% penicillin/ streptomycin (Pen/ Strep) (all products from ScienCell) for 24h at 37ºC at 5% CO_2. Next day selected wells were activated with 5 ng/ul of TGF-β per 100 µl (96 well plate) or 500 µl (24 well plate) of 0% FBS SteCell medium per well for 24h at 5% CO_2. After that cells were used for different experiments mentioned in the following sections. PSCs were used from a passage of 4-10.

2.9. PSCs Immunostaining

PSC seeded in 24 well plate were used for immunostaining. They were fixed with 500 µl/well of a acene:methanol mix (50:50) kept at -30ºC. Cells were incubated at -30C for 30 min. Then after the mix was removed they were stored at -80ºC. They were dried under warm air for approximately 30 min. Cells were washed with 155 mM PBS three times. Afterwards cells were washed with 2% bis(trimethylsilyl)acetamide (BSA) 155 mM PBS for 1h. Using hydrophobic A-PAP PEN (Daido Sangyo, Japan) the dry wells were circled near the walls several times until a circle could be seen. Each well was treated with 100 µl of anti-hintegrin α5 goat Ig (R&D systems, MN, USA) for 1h at room temperature in the dark. After wells were washed three times with 155 mM PBS. Each well was treated with 100 µl of anti-hintegrin α5 donkey anti-goat Ig (R&D systems, MN, USA) for 1h at room temperature in the dark. Then wells were washed three times with 155 mM PBS. The immunostaining was completed with the addition of 2 drops of Fluorshield with DAPI (Sigma-Aldrich, MO, USA). The plate was left overnight at room temperature in the dark. After the plate was investigated under EVOS (Invitrogen, CA, USA)

2.10. cDNA preparation

PSC RNA samples obtained through RNA extraction were used to obtained cDNA. cDNA was synthesized using standard products and protocols (Bio-Rad Laboratories B.V., Hercules, California, USA). Arktik Cycler (Thermofisher Scientific) was used or the synthesis with pre-designed protocols, provided by the manufacturers.

2.11. qPCR

The prepared cDNA was diluted to a final concentration of 5ng/mL using RNAse free water. P For each gene measured, a primer master mix was prepared consisting of 0.08 µl forward primer (15 mM),

0.08 µl backward primer (15mM), 4 µl SYBR Sensimix (Bioline Reagents, London, UK) and 1.86 µl RNAse-free water, adding up to a final volume of 6 µl for each well. 2 µl the primer master mix and cDNA were added in one well. The plate was sealed and centrifuged for 2 min before starting the qPCR conform standard protocols (C1000 thermal cycler Bio-Rad, CFX 384 RT system). αSMA, PDGFRβ, Col1α1 and ITGA5 are the genes tested in the study. Gene expression results were based on the Cq values of each result. They were calculated with Microsoft Excel (Microsoft Corporation, Redmond, WA). The genes tested in the study, their forward and reverse sequence are mentioned in the Table A1 (Appendix).

2.12. Microscopy

2.12.1. Uptake study

AV3-LNPs and sAV3-LNPs encapsulating total RNA of RAW-eGFP positive cells and 1% DiI were used in the uptake studies. PSC cells seeded in 96 well plate prepared as mentioned above were treated with 250 uM of LNPs dissolved in warm 0% FBS medium for 2 or 24h, incubated at 37ºC at 5% CO_2. After that time medium was exchanged. Cells were inspected using EVOS at 2h and 24h timepoints.

2.12.2. Transfection study

MAL-LNPs, AV3-LNPs and sAV3-LNPs encapsulating total RNA RAW-eGFP positive cells:eGFP mRNA (3:1 weight ratio) mix and 1% DiI, were used in the transfection studies. PSC cells seeded in 96 well plate prepared as mentioned above were treated with LNPs that corresponded to 100 or 250 ng of RNA mix dissolved in warm 0% FBS medium for 2 or 24h, incubated at 37ºC at 5% CO_2. After that time medium was exchanged. Cells were inspected using EVOS at 48 h timepoint.

2.13. Statistics

All graphs were made using GraphPad Prism Version 5.00 (GraphPad Software Inc., San Diego, CA). All values are expressed as a mean ± standard error of the mean (SEM). Statistical significance of the results was performed by a two-tailed unpaired student's t-test for comparison of two treatment groups. Differences were considered significant for a p-value of $*p < 0.05$, $**p < 0.01$, $***p < 0.001$, respectively

3. Results

3.1. LNPs optimization and characterization

The first step in creating LNPs that can target CAFs was to manufacture LNPs. To do that various factors such as flow rate, lipid:RNA volume ratio or presence of DiI dye were taken into consideration. They were characterized by measuring size, PDI, zeta potential and encapsulation efficiency.

Table 1. Size, PdI and encapsulation efficiency (EE) of prepared LNPs.

Sample Name	LNP components	Flow rate	Lipid:RNA volume ratio	DiI	Z-Ave	PdI	Zeta Potential	EE
		ml/min			d.nm		mV	%
No PEG	DSPC, cholesterol, MC3,	12	1:3	Yes	763.9	0.611	0.04	22.65
PEG	DSPC, cholesterol, MC3, PE-PEG	12	1:3	Yes	175.2	0.218	-0.02	43.35
MAL	DSPC, cholesterol, MC3, PE-PEG, DSPE-PEG-MAL	12	1:3	Yes	222.6	0.461	0.05	41.48
Filtered MAL	DSPC, cholesterol, MC3, PE-PEG, DSPE-PEG-MAL	12	1:3	Yes	431.7	0.459	0.03	13.78
Extruded MAL	DSPC, cholesterol, MC3, PE-PEG, DSPE-PEG-MAL	12	1:3	Yes	1265	0.498	-0.01	8.97
2 ml/min	DSPC, cholesterol, MC3, PE-PEG, DSPE-PEG-MAL	2	1:3	Yes	179.6	0.241	0.02	39.98
20 ml/min	DSPC, cholesterol, MC3, PE-PEG, DSPE-PEG-MAL	20	1:3	Yes	228.6	0.451	-0.03	40.76
1:5 ratio	DSPC, cholesterol, MC3, PE-PEG, DSPE-PEG-MAL	12	1:5	Yes	286.3	0.447	0.07	37.25
No DiI	DSPC, cholesterol, MC3, PE-PEG, DSPE-PEG-MAL	12	1:3	No	198.6	0.53	0.03	44.85

Zeta potential is similar for all LNPs. Size differs for various formulations. Formulation without any PEG-lipid had the highest size out of all formulations that were not additionally processed after the

formulation. After PEG-lipids are added the size is reduced to 175 nm for "PEG" formulation and to 223 nm for "MAL" formulation. In order to check if we can further reduce the size of the formulation "MAL" was either filtered through 400 nm and 200 nm syringe filter 3 times or it was extruded through 200 nm, 100 nm and 80 nm filters. Both formulations increased in size, filtered to 432 nm and extruded to 1265 nm. Decreased flow ratio (2ml/min) resulted in decreased size of 180 nm while increased flow rate of 20 ml/min resulted in size similar to the one created with 12 ml/min since it was 228 nm. Lipid:RNA volume ratio of 1:5 produced LNPs with a size of 286 which is higher from MAL formulation by 63 nm. While absence of DiI in formulation resulted in LNPs with 200 nm size. Additionally, "20 ml/min" and "1:5 ratio" LNPs experienced DiI loss. The characteristically pink color of the formulation faded after the dialysis (Figure 6-Appendix). Encapsulation efficiency of all formulations apart from "No PEG", "filtered MAL" and "Extruded MAL" was around 40 ± 4%. Those 3 formulations had a lower encapsulation efficiency with the lowest being 8.97 for "Extruded MAL".

3.2. LNPs size stability

To determine the size stability of created LNPs we measured the size of the formulations over the course of three weeks. Size was measured for the formulations that had size below 300 nm. In Table 2 we can see that all the formulations apart from "20min/ml" and "1:5 ratio" had similar size over the period of 3 weeks. For "20 ml/min" the LNPs increased in size from 228.6 nm in the first week to 347.3 nm in the third week. In contrast "1:5 ratio" LNPs decreased in size from 286.3 to 238.1 nm in the third week. PDI for "PEG" and "2ml/min" were 0.2 in the first week, at the third week it increased to 0.4 and 0.3 respectively. The other formulations started the first week with a PDI of 0.4 or 0.5 and stayed similar for the duration of the test. It was decided that formulations "MAL", "2ml/min" and "No DiI" will be used for further testing.

Table 2. Size stability of LNPs

	1 week		2 week		3 week	
Sample Name	**Z-Ave**	**PdI**	**Z-Ave**	**PdI**	**Z-Ave**	**PdI**
	d.nm		**d.nm**		**d.nm**	
PEG	175.2	0.2	192.4	0.4	168.5	0.4
MAL	222.6	0.5	218.1	0.3	227.1	0.3
2 ml/min	179.6	0.2	178.2	0.2	188.2	0.3
20 ml/min	228.6	0.5	271.8	0.5	347.3	0.4
1:5 ratio	286.3	0.4	242.6	0.6	238.1	0.5
No DiI	198.6	0.5	201.0	0.5	204.3	0.4

3.3. AV3 peptidomimetic conjugation to LNPs

For the LNPs to be able to target ITGα5 they needed to be conjugated with AV3. The initial conjugation was done with 10 molar excess of AV3, dissolved in DMSO, with regard to DSPC-PEG-MAL lipid. To analyze the effect of conjugation size, PDI, zeta potential and encapsulation efficiency were measured (Table 3). The size of LNPs after conjugation increases 3 times for AV3 and 2.5 times for sAV3 before it is purified by dialysis. After purification with dialysis the size increases further to 1836 nm for LNPs-AV3 and to 1129 nm for LNPs-sAV3. Along with the increase in size, PdI goes from 0.4 before conjugation to 0.9 after conjugation. Encapsulation efficiency for the LNPs-MAL formulation was 46.7%. After conjugation with AV3 or sAV3 it decreased to 41.4% and 42.3 % respectively.

Table 3. Size, PDI and encapsulation efficiency (EE) of conjugated LNPs

Sample Name	Conditions	Z-Ave [d.nm]	PdI	EE
		d.nm		%
LNPs-Mal	-	143.5	0.4	46.7
LNPs-AV3	Before dialysis	491.6	0.9	-
LNPs-sAV3	Before dialysis	408.4	0.9	-
LNPs-AV3	After dialysis	1836	0.5	41.4
LNPs-sAV3	After dialysis	1129	0.6	42.3

3.4. Optimization of LNP-peptidomimetic conjugation

In order to prevent LNPs sizable increase in size after conjugation molar excess of AV3 or sAV3 was reduced from 10 to 3. Three different purification methods were applied to created “MAL” LNPs: dialysis, spin down column and desalting column. Additionally, during conjugation TCEP was added to half of the investigated formulation for each condition. Addition of TCEP resulted in decreased LNPs size for all conditions. Spin down columns and dialysis without TCEP resulted with LNPs that had a size above 300 nm. With the inclusion of TCEP during the conjugation LNPs obtained from dialysis had the size of 277.1 nm, while for spin down column the size was still above 300 nm. Desalting columns resulted in the smallest size of 227.4 nm and PdI of 0.3. Zeta potential was similar for all conditions. Desalting column was used as a purification method for all future formulations.

Table 4. Effect of different post conjugation purification methods on LNPs size, PdI and Zeta Potential.

Sample Name	Purification	TCEP	Z-Ave [d.nm]	PdI	Zeta Potential
			d.nm		mV
Mal	-	-	426.8	0,4	0.01
Av3	-	-	301.6	0,5	-0.01
AV3	-	Yes	185.8	0,3	-0.07
AV3	Spinned down	-	318.0	0,4	0.02
AV3	Spinned down	Yes	307.4	0,3	-0.01
AV3	Dialised	-	321.4	0,4	0.05
AV3	Dialised	Yes	277.1	0,5	-0.05
AV3	Desalting column	Yes	227.4	0,3	0.08

After establishing optimal conjugation conditions three out of the formulations from Table 2 that were chosen for further testing i.e. “MAL”, “2 ml/min” and “No DiI”, were conjugated with AV3 or sAV3. First the size, PdI and zeta potential of the formulations before the conjugation were tested (Table 5). “MAL” and “No DiI” formulation had similar size to the one obtained previously in Table 2 with 217.3 and 199.5 respectively, while “2 ml/min” was 81.2 nm larger than previously obtained LNPs size. After conjugation with either AV3 or sAV3, size, PdI and zeta potential of the formulations were tested (Table 5) again. “MAL” grew in size by around 10 nm for AV3 and sAV3. For “2ml/min” LNPs were enlarged by 15.5 nm for AV3 and 39.8 nm, while “no DiI” formulation grew by 40.6 nm for AV3 and 12.8 for sAV3. PdI of “2ml/min” LNPs was 0.5, “no DiI” was 0.5 or 0.4 and “MAL” was 0.4 before conjugation and 0.3 after conjugation. Zeta potential for all formulations was around 0. Due to the changes in size for “2 ml/min” LNPs the formulations were made again and while “MAL” and “No DiI” LNPs were similar in size, the “2ml/min” LNPs had different size than both of previously created samples (Figure 7- Appendix). Due to the lack of reproducibility of “2ml/min” LNPs it was decided that further in vitro testing will be done with “MAL” LNPs.

Table 5. Size, PDI and Zeta Potential of chosen LNPs

Sample	Z-Ave	PdI	Zeta Potential	Conjugation	Z-Ave	PdI	Zeta Potential
	d.nm		mV		d.nm		mV
MAL (12 ml/min)	217.3	0.4	-0.04	AV3	227.4	0.3	0.08
				sAV3	226.5	0.3	0.05
2 ml/min	260.8	0.5	-0.04	AV3	276.2	0.5	0.06
				sAV3	309.6	0.5	0.07
no DiI	199.5	0.5	-0.04	AV3	240.1	0.4	-0.06
				sAV3	212.3	0.5	0.02

3.5. PSC activation and expression of ITGα5

In order to see if AV3 conjugated LNPs will be able to target PSC cells, the cells were tested to see if they express ITGα5 in increased quantity after activation. Immunostaining was used to assess how much ITGα5a is expressed in their quiescent and activated state. PSCs activation was done by TGF-β. The immunostaining was done after 24h of TGF-β treatment. The results are displayed in Figure 1. Representative microscopy photos Figure 1a) show that activated PSCs have more intense fluorescence signal than quiescent PSCs, which is also supported by the quantified fluorescence intensity data in Figure 1b). Additionally, PSCs activation was also investigated by measuring gene expression of quiescent and activated PSC. PSCs were activated with TGF-β. In order to confirm the activation of the cells genes were tested with qPCR: αSMA, PDGFRβ, Col1α1 and ITGA5. There is a significant difference in the expression of all considered genes (Figure 1c-f). In case of αSMA there is 7 times fold increase between quiescent and activated PSCs, for PDGFRβ and Col1α1 it was about 4 times difference with the increase of signal for activated PSC and for ITGA5 it was 3 times difference. Both test confirm the activation of PSCs and overexpression of ITGα5 on activated PSCs.

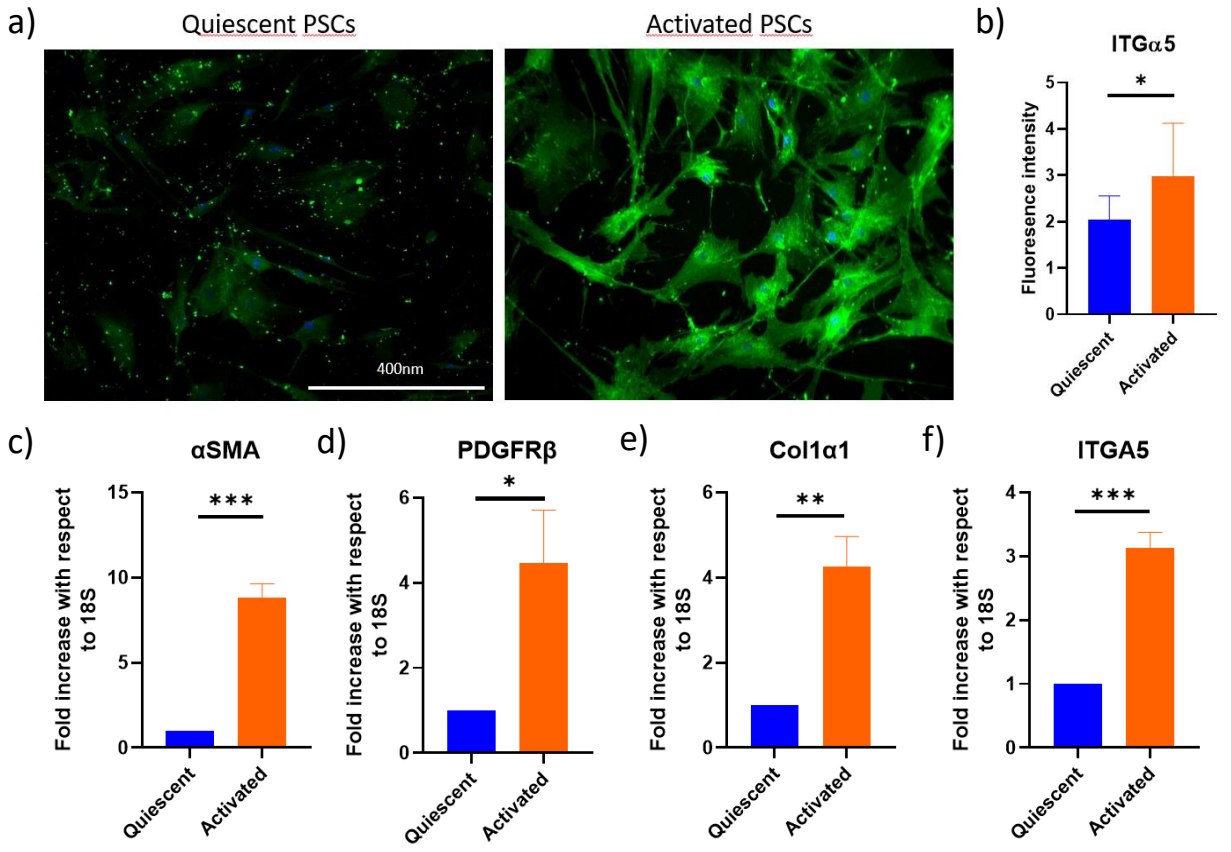

*Figure 8. a) Immunostaining of ITG5α on PSC cells in either quiescent or activated state. The blue signal shown on a photo represents DAPI stained nuclei and the green signal ITGα5. Quantified fluorescence intensity of ITGα5 f quiescent and activated PSC normalized with respect to number of cells. PSCs gene expression of c) αSMA, d) PDGFRβ, e) Col1α1 and f) ITGA5 normalized with respect to 18S. Data represent mean ± SEM for at least 3 independent experiments. Statistical analysis was performed by two tailed unpaired t-test. *p < 0.05, **p<0.01, ***p < 0.001.*

3.6. LNPs uptake by PSC cells

To evaluate the created formulations in vitro uptake studies are needed to confirm that the LNPs can target and enter the cells. For that purpose quiescent and activated PSCs were treated with 250 µM of LNPs-AV3 and LNPs-sAV3 for 24h. This formulations represent "MAL" conjugated with AV3 and sAV3 respectively. Figure 2 displays representative microscopy pictures for quiescent PSC cells. For all conditions there is no red DiI signal, which would indicate LNPs presence inside the cells. Figure 3 show representative microscopy pictures for activated PSC cells. Red DiI signal is visible for the PSC cells that were treated with LNPs-AV3. The signal is not present for control with are untreated cells or for PSC cells that were treated with LNPs-sAV3. It is worth to note that for control PSC cells in both Figure 2 and Figure 3 there were more cells than in wells that were treated with LNPs.

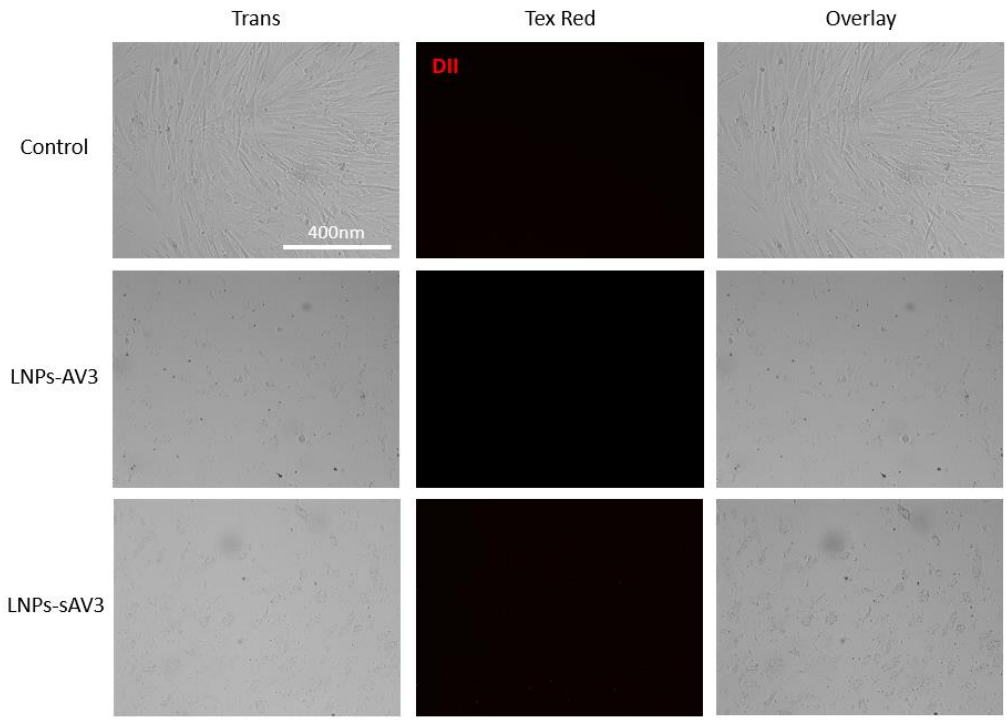

Figure 9. Representative microsocpy images of quiescent PSCs uptake of DII dye containing LNP-AV3 or LNP-sAV3 for 2h. The side headlines indicate the transfection conditions. For each condition the first picture displays just cells, the second one represetd just red DiI signal and the third picture reprsents overalsy of two previous pictures. The uptake study was performed using 250 µM of LNP-AV3 or LNP-sAV3.

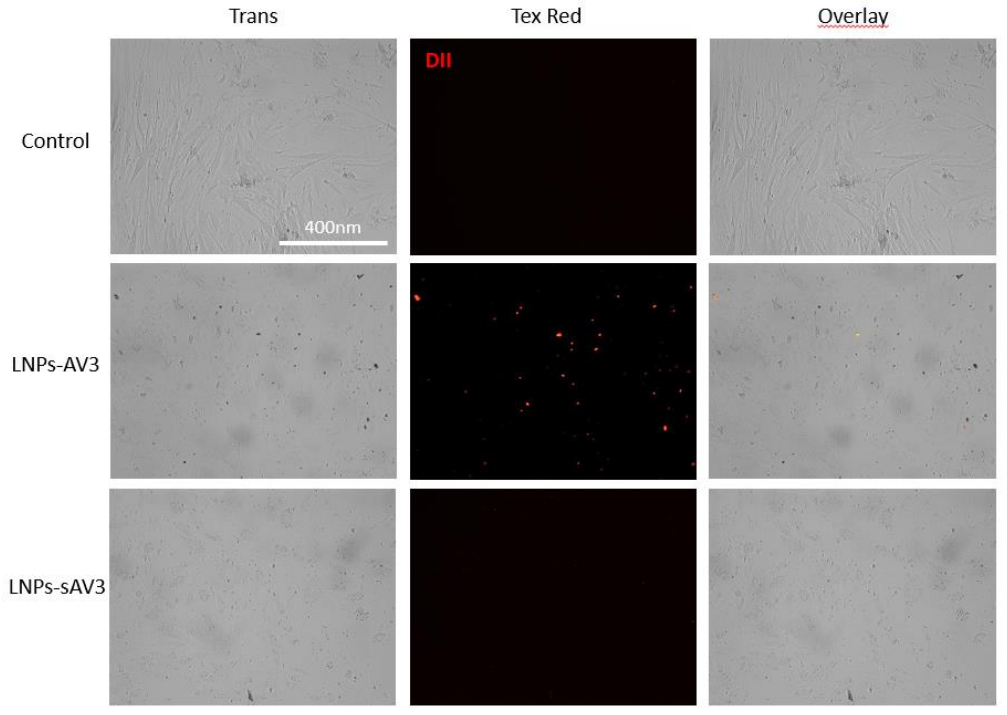

Figure 10. Representative microsocpy images of activated PSCs uptake of DII dye containing LNP-AV3 or LNP-sAV3 for 2h. The side headlines indicate the transfection conditions. For each condition the first picture displays just cells, the second one represetd just

red DiI signal and the third picture reprsents overalsy of two previous pictures. The uptake study was performed using 250 µM of LNP-AV3 or LNP-sAV3.

3.7. LNPs transfection of PSC cells

With the confirmation that created formulation are taken up by activated PSC, the quiescent and activated PSCs were transfected with LNPs-MAL, LNPs-AV3 and LNPs-sAV3. LNPs contained the mix of total RNA of RAW-eGFP positive cells and eGFP mRNA (3:1 weight ratio). Cells were transfected for 24h and pictures displayed in Figure 4 and Figure 5 display representative microscopy pictures taken 48h after transfection. GFP signal is the indication that the cells were transfected with help of LNPs. The results in Figure 4 show the effect that LNPs had on quiescent PSC. Red DiI signal and green GFP signal are visible only for PSC cells transfected with LNPs-sAV3. PSC cells transfected with LNPs-AV3 show negligible amount of green signal with no red signal, while cells transfected with LNPs-MAL show signal at all. The results of activated PSC transfection with LNPs are shown in Figure 5. Similarly to the results obtained for quiescent cells, on the pictures with cells that were transfected with LNPs-sAV3 there is red and green signal present. For LNPs-MAL again there was no signal detected. Alternatively in wells where cells were transfected with LNPs-AV3 red DiI signal and green GFP signal are both clearly visible.

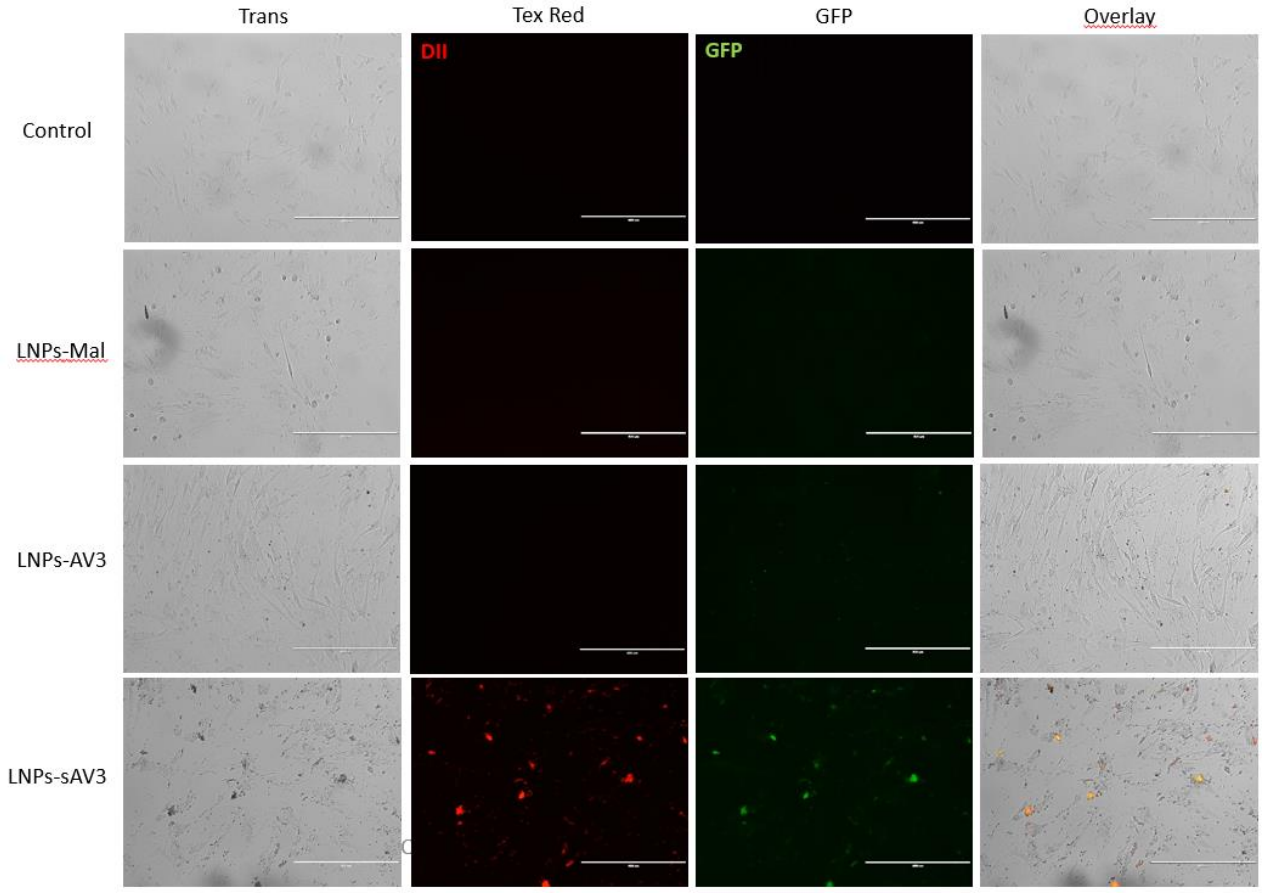

Figure 11. Representative microsocpy images of quiescent PSCs tarnsfection with LNPs-MAL, LNPs-AV3 or LNPs-sAV3 containing a mix of total RNA RAW-eGFP positive cells and eGFP mRNA (3:1) and DiI dye for 24h. The side headlines indicate the transfection conditions. For each condition the first picture displays just cells, the second one represetd just red DiI signal, the third picture reprsents mRNA eGFP signal and the fourth picture reprsents an overalsy of the three previous pictures. The uptake study was

performed using LNPs-MAL, LNPs-AV3 or LNPs-sAV3 in the amount that corresponds to 250 ng of total RNA RAW-eGFP positive cells and eGFP mRNA.

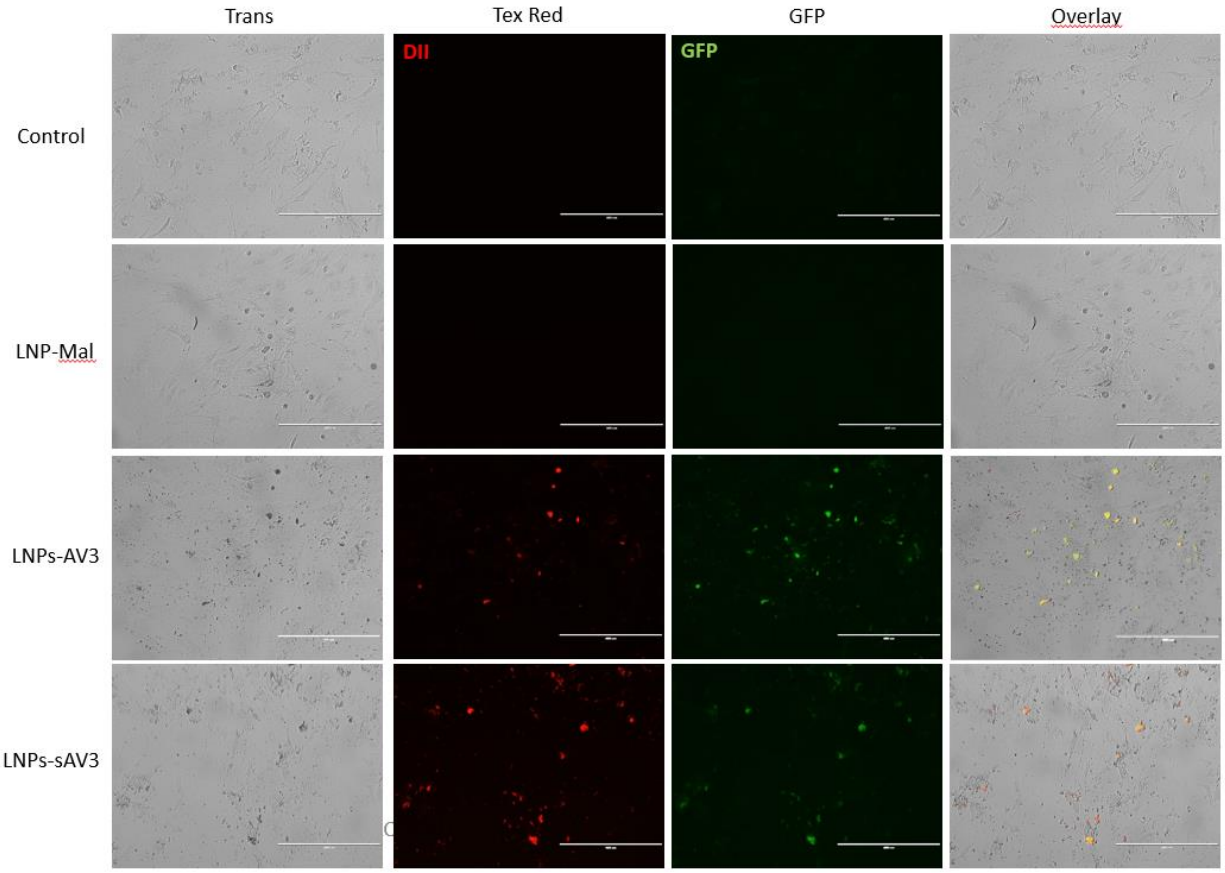

Figure 12. Representative microsocpy images of activated PSCs tarnsfection with LNPs-MAL, LNPs-AV3 or LNPs-sAV3 containing a mix of total RNA RAW-eGFP positive cells and eGFP mRNA (3:1) and DiI dye for 24h. The side headlines indicate the transfection conditions. For each condition the first picture displays just cells, the second one represetd just red DiI signal, the third picture reprsents mRNA eGFP signal and the fourth picture reprsents an overalsy of the three previous pictures. The uptake study was performed using LNPs-MAL, LNPs-AV3 or LNPs-sAV3 in the amount that corresponds to 250 ng of total RNA RAW-eGFP positive cells and eGFP mRNA

4. Discussion

Cancer is one of the deadliest diseases in the world. For decades tumors have been regarded to consist of only cancer cells. However, in recent years more components of tumor microenvironment have been found. It includes extracellular matrix as well as variety of cells. The cells that this particular study focuses on are cancer associated fibroblasts. They are involved in variety of pro-tumorigenic processes. Such as metastasis, angiogenesis, proliferation, survival and therapies resistance.[61] They achieve that largely by affecting other cells in the tumor microenvironment. That is why they are such an interesting target, because they affect variety of pro-tumorigenic processes. [62] And as we know current cancer therapies are connected with variety of side effects that decrease patients quality of life. Due to that alternative therapies are gaining more and more popularity. One of them are nucleic acid therapeutics. However due to their physical and chemical characteristics they cannot be administered on their own. They need to employ the use of a carrier in order to be able to reach and penetrate the surface of cells. One of the possible solutions are lipid nanoparticles, that has been shown to be able to encapsulate various nucleic acids and deliver them to the desired cells. [4][63]

In this study, we aimed to produce lipid nanoparticles that will be able to encapsulate nucleic acids and then deliver them to cancer associated fibroblasts. The first step to targeted delivery of nucleic acids to CAFs is design and production of a vessel that can safely transport and deliver the cargo. That is why the first experiments focused on the design and assessment of different conditions that have to be taken into the consideration when preparing lipid nanoparticles. During that experiment we looked into the composition of nanoparticles, effect of cationic dye, flow rates used during the microfluidic mixing as well as lipid:RNA volume ratio. Firstly we look into the composition of lipid nanoparticles. LNPs were created with the usage of DSPC, cholesterol, PE-PEG, MC3 and DSPE-PEG-MAL. Two formulations were prepared as a control. First did not have any PEG lipid "No PEG" and the second one used only PE-PEG as a PEG lipid. Obtained results show that "No PEG" formulation was noticeably larger than all other formulations that did contain PE-PEG lipid. This portrays that PEG lipids are necessary building blocks of LNPs, as they add stability to the formulation. [64][55][65] In the study done by Kalyanmar et al [66] it has been shown that the absence of PEG lipid resulted in LNPs with the size of over 1500 nm, while with the usage of PEG the size lowered to below 200 nm. Multiple other studies also report similar founding's. PEG lipid concentration can actually affect the size of the formulation. Although the most widely used concentration is 1.5 %. [67][68][69][70] This study shown that by increasing the PEG concertation to 3% or 5%, size of the nanoparticles can be further decreased. What is more the study showed that decreasing the cholesterol in favor of PEG is more efficient in size reduction than decreasing the helper lipid (DSPC) in favor of PEG. Lately more and more studies have been focused on the effect of different components of LNPs. In a study done by Alvarez-Benedicto at al. [71] helper lipids have been shown to affect the size, encapsulation efficiency, zeta potential, uptake and transection efficiency of the LNPs in different cell lines. The sizes varied between 100 to 250 nm, and encapsulation efficiency between 50% and 90%. Another component of LNPs that have been shown to affect their properties is cholesterol. In the study of Patel et al. [72] different cholesterol analogues has been tested to see the effects on LNPs properties and subsequently on in vitro studies conducted with them. They tested cholesterol with various modifications and as a results created LNPs, that possessed different size, encapsulation and transfection efficacy. The size varied between 100 and 200 nm, while encapsulation efficiency between 25% to 90%. That shows us that when it comes to the optimization of LNPs design there are a lot of factors that need to be taken into the consideration in the

future experiments as variety of them have effect, not only on size and encapsulation efficiency but also on their efficacy in vitro.

The importance of LNP composition can be seen with the results that were obtained for "MAL" formulation. This formulation was larger than "PEG" formulation by 47.4 nm (Table 1). This high increase in size was surprising looking at the fact that the added particle was a DSPE-PEG-maleimide and it made out only 0.03 % of the whole formulation. So as we can see even small changes to the LNPs composition can result in noticeable difference. In a study by Wang et al. [73] where they used DSPE-PEG as a PEG lipid the size of the particles depended on the helper lipid that was used. Aa a result attained sizes were between 150 nm to over 300 nm. For the DSPC the average size was above 250 nm. Lower sizes around 160 nm were obtained for DSPE and PC-98T helper lipid. Considering that even if in our experiment the usage of DSPE-PEG-maleimide resulted in an increased LNP size it is still comparable to other formulations with similar components that are found in the literature. Current formulation can be still further improved upon in future experiments by considering alternative lipids.

The lipid nanoparticles are not only affected by their components, there are other factors involved in the formulation process that play an important role on the final outcome. One of the factors taken into the consideration when it comes to LNPs fabrication is flow rate in a microfluidic device. Flow rate refers to the amount of liquid that is pushed through the whole device in a specific time. It is responsible for creating a chaotic mixing environment that allows for the optimal condition for creating LNPs. It has been shown by Roces at al. [74] that increase flow rate results in smaller LNPs, while decreased flow rate resulted in larger LNPs. Although the difference in size between 10 ml/min and 20 ml/min was not large. The same was reported by Webb et al. [75] That is why it was expected that the increase in flow rate might not results in significantly smaller LNPs. However, obtained results shown in Table 1, were contrary to mentioned studies. The "20 ml/min" formulation resulted in LNPs with similar size to the ones prepared with 12 ml/min flow rate with a difference of 6nm, while the formulation prepared with 2ml/min resulted in formulation smaller by 43 nm. However, later studies as presented in Figure A2, have shown that the size obtained with 2ml/min is not always the same, with one of the samples going up to 260.8 nm, while the other two formulations made with 2ml/min flow rate created LNPs with sizes larger or similar to LNPs made with 12 ml/min. That is why to check if increased flow rate would result in larger nanoparticles, more formulations made with the same parameters are need. Based on the obtained results 12 ml/min brings the most reproducible results out of all flow rates under the investigation.

Another factor checked was lipid:RNA volume ratio. It was shown by Roces at al. [74] that increased ratio can result in a lowered LNP size depending on its components. However, in the study done by Webb et al.[75] higher ratio resulted in a slightly increased size of nanoparticles. In our study, volume ratio of 1:5 did not result in a lowered size in comparison to 1:3 ratio, in fact it resulted in a formulation larger by 63.7 nm. The differences in flow ratio were not investigated further as the obtained results as well as the previously mentioned studies did not show a significant improvement in size of LNPs above 1:3 ratio.

All but one formulation was created with the usage of DiI dye. DiI was used in order to detect uptake of LNPs by PSCs. The formulation "No DiI" was created without the dye to see if the presence of DiI affects the LNPs. The data collected by me are not comparable to any other studies found in the literature since all the studies that deal with nucleic acid containing LNPs use nucleic acid conjugated

with fluorescent dye. They do not use separate substance for that purpose. [76][77][78] It was shown in the Table 1 and then in Table 5 and Figure A2 that the formulations without DiI ("No DiI") are about 20 nm smaller than the formulations that have the DiI and are made with the same conditions. The possible reason for this difference might come from the fact that DiI is a cationic lipophilic dye [79][80] and MC3 is an ionizable lipid that becomes protonated at lowered pH. In the cation-cation interactions the charge of the particles leads to the creation of repulsive forces. [81] That might be also occurring between positively charged amino group on the DiI and nitrogen found on the MC3. Considering that during the formulation process when ethanol phase containing MC3 and DiI is chaotically mixed with the RNA solution, with pH 4. The change in size might be also attributed to the addition of another substance to the lipid layer of the LNPs. DiI possess two lipophilic hydrocarbon side chains made out of eighteen carbons that work themselves into the lipids in the lipid nanoparticles. [82][83] For further studies it might be more advisable to obtain mRNA molecules already conjugated with dyes for the uptake studies, rather than use a lipophilic dye that increases the size of the formulation. However, for this study DiI was an acceptable starting point due to its accessibility, low toxicity and photostability[83].

When we look at the size stability results (Table 2) we see that all but two formulations remained similar in size and PdI over the course of 3 weeks. "20 ml/min" LNPs grew in size by 118.7 nm, while "1:5 ratio" LNPs decreased in size by 48.2 nm. The growth in size might be caused by the difference in charge between the inside and outside of LNPs, due to which more water molecules travel inside the LNPs. The decrease in membrane size is more difficult to explain as active transport of water against concentration gradient is not a viable option as created LNPs were not equipped with required membrane structures such as SGLT1 or GLUT2. [84] However, as it was mentioned before these formulation did not behave similar to other comparable formulation in the literature [74][75]. Moreover, as it was shown in Figure 2A when the "2 ml/min" LNPs were formulated again it displayed different properties. What is also worth to notice is that during formulation process after dialysis it was noticed that "20ml/min" and "1:5 ratio" formulations displayed visible loss of color in the formulation where said color should have remained prominent as it was prepared with intense DiI color (Figure A1). That might suggest that said LNPs were not stable. It might be that the used microfluidic chip was used too many times before those formulations were made and as a result mixing was not as efficient as it should have been and resulted in unstable LNPs.

In general created lipid nanoparticles were stable, able to encapsulate used RNA and results in size that although higher than in literature were comparable when taking into account the usage of additional PEG-lipid with attached maleimide. Those particles were then taken for the next step in the preparation of CAF targeting LNPs, that is AV3/sAV3 conjugation. The first attempts at AV3 conjugation (Table 3) resulted in significant increase in the nanoparticles size. After conjugation but before the purification the LNPs were already bigger than 400 nm and after the dialysis they were larger than 1000 nm. There were a few factor that could have possibly affect the size. First being the amount of molar excess of AV3 that was used with respect to the amount of DSPE-PEG-MAL used. That is why molar excess was reduced from 10 to 3. That resulted in a LNPs that decreased in size by almost 200 nm (Table 4). However, the size was still relatively high. That is why the next step in further size reduction was usage of TCEP. TCEP is a common disulfide bond reducing agent. It has been shown to assist in the thiol-maleimide reaction by making more thiol group available for the conjugation. [85][86] In this study the usage of TCEP resulted in an even further reduction in size for the created LNPs. Before the purification LNPs had the size of 185.8 nm (Table 4). After successful reduction in size next step was to investigate

different purification techniques, as previously used dialysis resulted in significant increase in size (Table3). In this experiment 3 different types of purification method have been under the investigation: dialysis, spin column and desalting column. While this time dialysis did not result in as significant growth as previously, obtained size was still higher than the desalting column which generated the smallest size increase with respect to the size obtained prior to the purification. With that experiment we were able to optimize the conjugation process, by adjusting the three above mentioned factors: molar excess, TCEP usage and purification method.

Two factors that did not change values through different optimization steps were zeta potential and encapsulation efficiency. Zeta potential informs us about the charge of created particles. For all formulations zeta potential was measured to be around 0 mV. Making this particles neutral in charge. Encapsulation efficacy is a measure of how much nucleic acid were inside LNPs. For all, but "No PEG" formulation it was around 40%, while for the "No PEG formulation it was 22.65 %. This difference might be connected with the fact that as it was shown above PEG lipid help in LNPs stabilization. Without it RNA might have leaked out of the formulation after dialysis when it was at pH 7 and MC3 was no longer active and connected with RNA. As mentioned all other formulations had a comparable encapsulation efficiency, which was maintained after conjugation. When looking at literature this encapsulation efficiency is on the lower side. However in the study done by the Alvarez-Benedicto at al. [71] it was shown that usage of different helper lipids results in various RNA encapsulation from 50% to 90%. Looking at that we can see that with the further optimization of LNP design it is possible to adjust the encapsulation efficiency of lipid nanoparticles.

In order to make sure that we will be able to test the uptake and transfection of produced LNPs, we investigated the effects of activation of PSCs by TGF-β. In order to do that first we checked the expression of ITGα5 on quiescent and activated PSCs. It was shown by the Figure 9a-b that activated cells expressed more ITGα5 than quiescent cells. This shown that LNPs conjugated with AV3 should be able to target and interact with PSCs as AV3 targets the ITGα5 that according to study done by Kuninty et al. [2] is overexpressed on activated PSCs. The second experiment investigated the gene expression of four genes: αSMA, PDGFRβ, Col1α1 and ITGA5. αSMA is a member of actin family that has effect on structure, integrity and motility of fibroblasts.[87] While it is not an exclusive fibroblast marker, it is up regulated in activated fibroblasts, where ECM is being actively deposited, like in case of tumor microenvironment. [88][89] That is why more markers have to be investigated to make sure that the cells under investigation are activated fibroblast and are not other cells that also overexpress this gene. In the results obtained in this study αSMA is upregulated in activated cells in comparison to quiescent cells. PDGFRβ are receptors that are located on fibroblasts. They are commonly used for CAF detection, which is indicated by the up regulation of the gene in question [87][90][91]. The data obtained from performed experiments show that the gene corresponding to this receptor is upregulated in activated PSC in comparison to quiescent PSCs. Col1α1 is another factor upregulated in cancer associated fibroblasts, as fibroblasts are involved in ECM production where collagen is one of the building blocks. [92][93][94] ITGA5 gene upregulation is expected as it was mentioned before ITGα5 is over expressed in CAFs. For both, Col1α1 and ITGA5, genes were upregulated. In conclusion all of the genes investigated in this experiment had higher gene expression in PSC treated with TGF-β then in quiescent cells. That confirms that the usage of TGF-β results in activated PSCs that have increased ITGα5 expression. Which in turn shows that PSCs can be used to evaluate uptake and transfection studies of AV3 conjugated LNPs

The confirmation that PSCs are a suitable target for the demonstration of uptake and transfection of created LNPs enabled the in vitro studies. The uptake studies were performed with the usage of total RNA of RAW-eGFP positive cells and DiI dye. The presences of red fluorescence signal inside the cells captured on photos indicates presence of DiI filled LNPs inside the PSCs. The studies, demonstrated with the presence of red DiI signal that LNPs-AV3 target activated PSCs (Figure 10) while the absence of red signal depicted that they do not target quiescent cells (Figure 9). The same study showed that LNPs-sAV3 does not target PSC in either of states. Considering that LNPs-AV3 are capable of targeting activated PSC transfection studies followed. Here instead of using just total RNA of RAW-eGFP positive cells we used a mix of total RNA of RAW-eGFP positive cells:eGFP mRNA (3:1 weight ratio) as well as DiI. The presence of green signal represents a successful transfection as the green signal is created by the presence of GFPs that were made from the eGFP mRNA molecules. Cells were transfected for 24h and the results were obtained at 48h timepoint. In this study we included additional control of LNPs-MAL, which is an unconjugated "MAL" formulation. The transfection study confirmed that LNPs-AV3 target activated PSCs and not the quiescent ones, as green signal was visible only for cells activated with TGF-β. For LNP-sAV3 formulation targeted both types of cells which is in contrast with the results obtained with the uptake studies where they did not target any cells. As sAV3 is scrambles AV3, the sequence might target some alternative part of ITGα5, which would explain the presence of signal inside the cells. Due to that ambiguity and the fact that scrambled AV3 still might target in some way ITGα5, other controls might be more reliable, like the additional control used for this study: LNPs-MAL. Said control show no transfection or uptake by the quiescent (Figure 11) or activated cells (Figure 12), as both did not displayed red or green signal. That data shows that the usage of AV3 peptidomimetic allows for the targeting of activated PSCs as well as the fact that produced LNPs are capable of delivering nucleic acids to the cells. However, this experiment should be repeated again as several of the pictures in Figure 11 and 12 show that the cells are distressed and in some wells the confluency of cells decreased noticeably by the last day of the experiment. That is most likely cause by the usage of 0% FBS cell culture medium over the several days of the experiment. FBS is a vital part of the medium as it is growth supplement that facilitates cell growth and proliferation. [95] In transfection experiment cells were in a medium without FBS for 5 days, that is why for the future experiments it might be more beneficial to switch to using 2% FBS medium after transfection is completed which would reduce the that time from 5 to 3-4 days, depending on the length of the transfection.

5. Conclusions

In this study we were able to produce lipid nanoparticles that can encapsulate nucleic acids and deliver them to targeted cells. Conducted experiments demonstrated that LNPs characteristics are dependent on production factors such as flow ratio or lipid:RNA ratio. Another important factor impacting nanoparticle properties is LNP composition. The addition of DSPE-PEG resulted in bigger LNPs, while absence of DiI resulted in smaller LNPs. Conjugation and purification procedure also play an important role in optimizing LNP properties, where the optimal conditions include three times molar excess of AV3, inclusion of TCEP during conjugation and usage of desalting column for purification. Taking all different factors into consideration we managed to produce LNPs with an acceptable size that were able to encapsulate nucleic acids. Created formulations were tested on PSCs treated with TGF-β. Due to that cells became activated and overexpressed ITGα5, which is the targeted by AV3 conjugated to LNPs. In vitro studies confirmed that LNPs-AV3 are being taken up by activated cells and not by quiescent ones. The transfection study showed that LNPs-AV3 are capable of delivering RNA to the activated PSCs. To conclude, we were able to produce LNPs that target activated fibroblast to deliver RNA.

6. Future Outlook

The goal of this thesis was to create targeted lipid nanoparticles that will be able to carry and deliver nucleic acids to cancer associated fibroblasts. This study presented that it possible to encapsulate nucleic acids in lipid nanoparticles that are able to target activated fibroblasts. It gave the basis for further development of this delivery platform. The ideal future end outcome of this study would be to obtain small lipid nanoparticles that will be able to encapsulate more than 90% of used nucleic acid. Those LNPs would then be loaded with a therapeutic nucleic acid that enables deactivation of cancer associated fibroblast to halt the pro-tumorigenic effect of CAFs in TME. The delivery and usage of nucleic acid therapeutics could possibly assist traditional therapeutics to increase efficacy of the treatment without increasing side effects or adding additional ones. While it is ideal outcome, there is still a lot of work to be done before we can bring the platform produced in this study to this ideal end point. However, this study gives a starting point for creating a delivery vesicle that will be able to deliver nucleic acid therapeutics. There are several avenues that can be explored to bring this study closer to the desired results.

One of them is adjusting the LNP composition. It can be done by testing different helper lipids. One of the promising lipids that has been shown in several studies to have helped achieve good properties is DOPE.[64][71] However, several helper lipid should be taken into consideration with respect to our composition design. Apart from helper lipid it might be also beneficial to consider different PEG lipid in place of PE-PEG. In several studies it has been shown that PEG lipid change can result in smaller size and/or better encapsulation efficiency. Other factor that can be used to improve LNPs are different cholesterol derivatives. Moreover, another idea worth exploring is trying different molar amounts of DSPE-PEG-maleimide. As it was presented before (Table 1) with the addition of this lipid the size of LNPs grew noticeably. That is why it might be beneficial to examine lower lipid concentrations. With this experiment it will be important to not only look at the size and encapsulation efficiency by also on the uptake of the LNPs, which can be monitored with microscopy and flow cytometry.

After showing that we are able to encapsulate and deliver nucleic acids with created formulation it would be advisable to look into N/P ratio and how it affects LNP parameters. N/P ratio is a ratio of ionizable lipid nitrogen group and phosphate group of nucleic acid. N/P ratio has been shown to have effect on size and encapsulation efficacy of LNPs. [68][73][96] In study described in this thesis we were unable to regulate N/P ratio as all of the formulations had total RNA of RAW-eGFP positive cells. Due to the fact that we were using total RNA we did not know the amount of basepairs. Therefore, we were unable to calculate the amount of phosphate group present in the formulation which resulted in unknown N/P ratio. In the future experiments where the whole nucleic acid load will be made of know RNA then it will be possible to use N/P ratio as additional factor in LNPs design.

For the future uptake studies I would recommend to use LNPs with nucleic acids that are conjugated to the dye, instead of using DiI. As we could see that the size of LNPs containing the dye is approximately 20 nm higher before conjugation. It was noticed that cell confluency at the end of in vitro experiments is lowered in comparison to the beginning, additionally cells often look stressed by the end of the experiment. For all in vitro studies I would recommend switching the medium to 2% FBS one after treatment with LNPs instead of leaving the cells on 0% FBS medium, to investigate if cell condition can be improved to provide more advantageous conditions.

7. References

[1] "Cancer." https://www.who.int/news-room/fact-sheets/detail/cancer.

[2] P. R. Kuninty *et al.*, "ITGA5 inhibition in pancreatic stellate cells attenuates desmoplasia and potentiates efficacy of chemotherapy in pancreatic cancer," *Sci. Adv.*, vol. 5, no. 9, p. eaax2770, 2019, doi: 10.1126/sciadv.aax2770.

[3] K. Sridharan and N. J. Gogtay, "Therapeutic nucleic acids: current clinical status.," *Br. J. Clin. Pharmacol.*, vol. 82, no. 3, pp. 659–672, Sep. 2016, doi: 10.1111/bcp.12987.

[4] J. A. Kulkarni *et al.*, "The current landscape of nucleic acid therapeutics," *Nat. Nanotechnol.*, vol. 16, no. 6, pp. 630–643, 2021, doi: 10.1038/s41565-021-00898-0.

[5] H. Sung *et al.*, "Global Cancer Statistics 2020: GLOBOCAN Estimates of Incidence and Mortality Worldwide for 36 Cancers in 185 Countries," *CA. Cancer J. Clin.*, vol. 71, no. 3, pp. 209–249, 2021, doi: https://doi.org/10.3322/caac.21660.

[6] R. L. Siegel, K. D. Miller, H. E. Fuchs, and A. Jemal, "Cancer statistics, 2022," *CA. Cancer J. Clin.*, vol. 72, no. 1, pp. 7–33, 2022.

[7] J.-X. Hu *et al.*, "Pancreatic cancer: A review of epidemiology, trend, and risk factors.," *World J. Gastroenterol.*, vol. 27, no. 27, pp. 4298–4321, Jul. 2021, doi: 10.3748/wjg.v27.i27.4298.

[8] T. S. Deisboeck, Z. Wang, P. Macklin, and V. Cristini, "Multiscale Cancer Modeling," *Annu. Rev. Biomed. Eng.*, vol. 13, no. 1, pp. 127–155, 2011, doi: 10.1146/annurev-bioeng-071910-124729.

[9] H. H. Q. Heng, J. B. Stevens, S. W. Bremer, G. Liu, B. Y. Abdallah, and C. J. Ye, "Evolutionary Mechanisms and Diversity in Cancer," vol. 112, D. B. T.-A. in C. R. Gisselsson, Ed. Academic Press, 2011, pp. 217–253.

[10] E. Henke, R. Nandigama, and S. Ergün, "Extracellular Matrix in the Tumor Microenvironment and Its Impact on Cancer Therapy," *Front. Mol. Biosci.*, vol. 6, 2020, doi: 10.3389/fmolb.2019.00160.

[11] C. Walker, E. Mojares, and A. Del Río Hernández, "Role of Extracellular Matrix in Development and Cancer Progression," *Int. J. Mol. Sci.*, vol. 19, no. 10, 2018, doi: 10.3390/ijms19103028.

[12] J. Iijima, K. Konno, and N. Itano, "Inflammatory Alterations of the Extracellular Matrix in the Tumor Microenvironment," *Cancers (Basel).*, vol. 3, no. 3, pp. 3189–3205, 2011, doi: 10.3390/cancers3033189.

[13] H. M. Micek, M. R. Visetsouk, K. S. Masters, and P. K. Kreeger, "Engineering the Extracellular Matrix to Model the Evolving Tumor Microenvironment," *iScience*, vol. 23, no. 11, p. 101742, 2020, doi: https://doi.org/10.1016/j.isci.2020.101742.

[14] D. A. Senthebane *et al.*, "The Role of Tumor Microenvironment in Chemoresistance: 3D Extracellular Matrices as Accomplices," *Int. J. Mol. Sci.*, vol. 19, no. 10, 2018, doi: 10.3390/ijms19102861.

[15] W. H. Fridman, F. Pagès, C. Sautès-Fridman, and J. Galon, "The immune contexture in human tumours: impact on clinical outcome," *Nat. Rev. Cancer*, vol. 12, no. 4, pp. 298–306, 2012, doi: 10.1038/nrc3245.

[16] D. J. Campbell and M. A. Koch, "Treg cells: patrolling a dangerous neighborhood," *Nat. Med.*, vol.

17, no. 8, pp. 929–930, 2011, doi: 10.1038/nm.2433.

[17] N. M. Anderson and M. C. Simon, “The tumor microenvironment,” *Curr. Biol.*, vol. 30, no. 16, pp. R921–R925, 2020, doi: https://doi.org/10.1016/j.cub.2020.06.081.

[18] I. Terrén, A. Orrantia, J. Vitallé, O. Zenarruzabeitia, and F. Borrego, “NK Cell Metabolism and Tumor Microenvironment,” *Front. Immunol.*, vol. 10, 2019, doi: 10.3389/fimmu.2019.02278.

[19] D. I. Gabrilovich, S. Ostrand-Rosenberg, and V. Bronte, “Coordinated regulation of myeloid cells by tumours,” *Nat. Rev. Immunol.*, vol. 12, no. 4, pp. 253–268, 2012, doi: 10.1038/nri3175.

[20] L. Yang and Y. Zhang, “Tumor-associated macrophages: from basic research to clinical application,” *J. Hematol. Oncol.*, vol. 10, no. 1, p. 58, 2017, doi: 10.1186/s13045-017-0430-2.

[21] Y. Chen, Y. Song, W. Du, L. Gong, H. Chang, and Z. Zou, “Tumor-associated macrophages: an accomplice in solid tumor progression,” *J. Biomed. Sci.*, vol. 26, no. 1, p. 78, 2019, doi: 10.1186/s12929-019-0568-z.

[22] P. Pathria, T. L. Louis, and J. A. Varner, “Targeting Tumor-Associated Macrophages in Cancer,” *Trends Immunol.*, vol. 40, no. 4, pp. 310–327, 2019, doi: https://doi.org/10.1016/j.it.2019.02.003.

[23] K. Louault, R.-R. Li, and Y. A. DeClerck, “Cancer-Associated Fibroblasts: Understanding Their Heterogeneity.,” *Cancers (Basel).*, vol. 12, no. 11, Oct. 2020, doi: 10.3390/cancers12113108.

[24] Q. Ping *et al.*, “Cancer-associated fibroblasts: overview, progress, challenges, and directions,” *Cancer Gene Ther.*, vol. 28, no. 9, pp. 984–999, 2021, doi: 10.1038/s41417-021-00318-4.

[25] E. Sahai *et al.*, “A framework for advancing our understanding of cancer-associated fibroblasts,” *Nat. Rev. Cancer*, vol. 20, no. 3, pp. 174–186, 2020, doi: 10.1038/s41568-019-0238-1.

[26] S. Su *et al.*, “CD10+GPR77+ Cancer-Associated Fibroblasts Promote Cancer Formation and Chemoresistance by Sustaining Cancer Stemness,” *Cell*, vol. 172, no. 4, pp. 841-856.e16, 2018, doi: https://doi.org/10.1016/j.cell.2018.01.009.

[27] M. E. Fiori, S. Di Franco, L. Villanova, P. Bianca, G. Stassi, and R. De Maria, “Cancer-associated fibroblasts as abettors of tumor progression at the crossroads of EMT and therapy resistance,” *Mol. Cancer*, vol. 18, no. 1, p. 70, 2019, doi: 10.1186/s12943-019-0994-2.

[28] S. Álvarez-Teijeiro *et al.*, “Factors Secreted by Cancer-Associated Fibroblasts that Sustain Cancer Stem Properties in Head and Neck Squamous Carcinoma Cells as Potential Therapeutic Targets,” *Cancers (Basel).*, vol. 10, no. 9, 2018, doi: 10.3390/cancers10090334.

[29] X. Chen and E. Song, “Turning foes to friends: targeting cancer-associated fibroblasts,” *Nat. Rev. Drug Discov.*, vol. 18, no. 2, pp. 99–115, 2019, doi: 10.1038/s41573-018-0004-1.

[30] M. Augsten *et al.*, “Cancer-Associated Fibroblasts Expressing CXCL14 Rely upon NOS1-Derived Nitric Oxide Signaling for Their Tumor-Supporting Properties,” *Cancer Res.*, vol. 74, no. 11, pp. 2999–3010, 2014, doi: 10.1158/0008-5472.CAN-13-2740.

[31] N. Cohen *et al.*, “Fibroblasts drive an immunosuppressive and growth-promoting microenvironment in breast cancer via secretion of Chitinase 3-like 1,” *Oncogene*, vol. 36, no. 31, pp. 4457–4468, 2017, doi: 10.1038/onc.2017.65.

[32] L. Monteran and N. Erez, “The Dark Side of Fibroblasts: Cancer-Associated Fibroblasts as

Mediators of Immunosuppression in the Tumor Microenvironment," *Front. Immunol.*, vol. 10, 2019, doi: 10.3389/fimmu.2019.01835.

[33] R. A. Flavell, S. Sanjabi, S. H. Wrzesinski, and P. Licona-Limón, "The polarization of immune cells in the tumour environment by TGFβ," *Nat. Rev. Immunol.*, vol. 10, no. 8, pp. 554–567, 2010, doi: 10.1038/nri2808.

[34] B. Li, G. Pei, J. Yao, Q. Ding, P. Jia, and Z. Zhao, "Cell-type deconvolution analysis identifies cancer-associated myofibroblast component as a poor prognostic factor in multiple cancer types," *Oncogene*, vol. 40, no. 28, pp. 4686–4694, 2021, doi: 10.1038/s41388-021-01870-x.

[35] E. Elyada *et al.*, "Cross-Species Single-Cell Analysis of Pancreatic Ductal Adenocarcinoma Reveals Antigen-Presenting Cancer-Associated Fibroblasts.," *Cancer Discov.*, vol. 9, no. 8, pp. 1102–1123, Aug. 2019, doi: 10.1158/2159-8290.CD-19-0094.

[36] D. Wu *et al.*, "Polymers with controlled assembly and rigidity made with click-functional peptide bundles," *Nature*, vol. 574, no. 7780, pp. 658–662, 2019, doi: 10.1038/s41586-019-1683-4.

[37] V. MacDonald, "Chemotherapy: managing side effects and safe handling.," *Can. Vet. J. = La Rev. Vet. Can.*, vol. 50, no. 6, pp. 665–668, Jun. 2009.

[38] Q.-Y. Zhang, F.-X. Wang, K.-K. Jia, and L.-D. Kong, "Natural Product Interventions for Chemotherapy and Radiotherapy-Induced Side Effects," *Front. Pharmacol.*, vol. 9, 2018, doi: 10.3389/fphar.2018.01253.

[39] T. R. Damase, R. Sukhovershin, C. Boada, F. Taraballi, R. I. Pettigrew, and J. P. Cooke, "The Limitless Future of RNA Therapeutics," *Front. Bioeng. Biotechnol.*, vol. 9, 2021, doi: 10.3389/fbioe.2021.628137.

[40] H. Zogg, R. Singh, and S. Ro, "Current Advances in RNA Therapeutics for Human Diseases," *Int. J. Mol. Sci.*, vol. 23, no. 5, 2022, doi: 10.3390/ijms23052736.

[41] C. Rinoldi *et al.*, "Nanotechnology-Assisted RNA Delivery: From Nucleic Acid Therapeutics to COVID-19 Vaccines," *Small Methods*, vol. 5, no. 9, p. 2100402, 2021, doi: https://doi.org/10.1002/smtd.202100402.

[42] J. C. Kaczmarek, P. S. Kowalski, and D. G. Anderson, "Advances in the delivery of RNA therapeutics: from concept to clinical reality," *Genome Med.*, vol. 9, no. 1, p. 60, 2017, doi: 10.1186/s13073-017-0450-0.

[43] S. Zhou, W. Chen, J. Cole, and G. Zhu, "Delivery of nucleic acid therapeutics for cancer immunotherapy," *Med. Drug Discov.*, vol. 6, p. 100023, 2020, doi: https://doi.org/10.1016/j.medidd.2020.100023.

[44] A. K. Iyer, Z. Duan, and M. M. Amiji, "Nanodelivery Systems for Nucleic Acid Therapeutics in Drug Resistant Tumors," *Mol. Pharm.*, vol. 11, no. 8, pp. 2511–2526, Aug. 2014, doi: 10.1021/mp500024p.

[45] P. Ghasemiyeh and S. Mohammadi-Samani, "Solid lipid nanoparticles and nanostructured lipid carriers as novel drug delivery systems: applications, advantages and disadvantages.," *Res. Pharm. Sci.*, vol. 13, no. 4, pp. 288–303, Aug. 2018, doi: 10.4103/1735-5362.235156.

[46] L. Sercombe, T. Veerati, F. Moheimani, S. Y. Wu, A. K. Sood, and S. Hua, "Advances and Challenges of Liposome Assisted Drug Delivery.," *Front. Pharmacol.*, vol. 6, p. 286, 2015, doi:

10.3389/fphar.2015.00286.

[47] G. A. Koning and G. Storm, “Targeted drug delivery systems for the intracellular delivery of macromolecular drugs.,” *Drug Discov. Today*, vol. 8, no. 11, pp. 482–483, Jun. 2003, doi: 10.1016/s1359-6446(03)02699-0.

[48] J. M. Metselaar and G. Storm, “Liposomes in the treatment of inflammatory disorders.,” *Expert Opin. Drug Deliv.*, vol. 2, no. 3, pp. 465–476, May 2005, doi: 10.1517/17425247.2.3.465.

[49] S. Hua and S. Y. Wu, “The use of lipid-based nanocarriers for targeted pain therapies.,” *Front. Pharmacol.*, vol. 4, p. 143, Nov. 2013, doi: 10.3389/fphar.2013.00143.

[50] B. N. Aldosari, I. M. Alfagih, and A. S. Almurshedi, “Lipid Nanoparticles as Delivery Systems for RNA-Based Vaccines,” *Pharmaceutics*, vol. 13, no. 2, 2021, doi: 10.3390/pharmaceutics13020206.

[51] X. Cheng and R. J. Lee, “The role of helper lipids in lipid nanoparticles (LNPs) designed for oligonucleotide delivery,” *Adv. Drug Deliv. Rev.*, vol. 99, pp. 129–137, 2016, doi: https://doi.org/10.1016/j.addr.2016.01.022.

[52] C. Hald Albertsen, J. A. Kulkarni, D. Witzigmann, M. Lind, K. Petersson, and J. B. Simonsen, “The role of lipid components in lipid nanoparticles for vaccines and gene therapy,” *Adv. Drug Deliv. Rev.*, vol. 188, p. 114416, 2022, doi: https://doi.org/10.1016/j.addr.2022.114416.

[53] X. Han *et al.*, “An ionizable lipid toolbox for RNA delivery,” *Nat. Commun.*, vol. 12, no. 1, p. 7233, 2021, doi: 10.1038/s41467-021-27493-0.

[54] D. Habrant *et al.*, “Design of Ionizable Lipids To Overcome the Limiting Step of Endosomal Escape: Application in the Intracellular Delivery of mRNA, DNA, and siRNA,” *J. Med. Chem.*, vol. 59, no. 7, pp. 3046–3062, Apr. 2016, doi: 10.1021/acs.jmedchem.5b01679.

[55] R. N. Kularatne, R. M. Crist, and S. T. Stern, “The Future of Tissue-Targeted Lipid Nanoparticle-Mediated Nucleic Acid Delivery,” *Pharmaceuticals*, vol. 15, no. 7, 2022, doi: 10.3390/ph15070897.

[56] M. Schlich *et al.*, “Cytosolic delivery of nucleic acids: The case of ionizable lipid nanoparticles,” *Bioeng. \& Transl. Med.*, vol. 6, no. 2, p. e10213, 2021, doi: https://doi.org/10.1002/btm2.10213.

[57] F. Ferraresso, A. W. Strilchuk, L. J. Juang, L. G. Poole, J. P. Luyendyk, and C. J. Kastrup, “Comparison of DLin-MC3-DMA and ALC-0315 for siRNA Delivery to Hepatocytes and Hepatic Stellate Cells,” *Mol. Pharm.*, vol. 19, no. 7, pp. 2175–2182, Jul. 2022, doi: 10.1021/acs.molpharmaceut.2c00033.

[58] A. Snow, L. Lin, S. A. Hunsucker, Y. Wang, R. Liu, and P. M. Armistead, “Development of a mRNA Lipid Nanoparticle (mRNA-LNP) Cancer Vaccine to Prevent Leukemia Relapse after Stem Cell Transplant,” *Blood*, vol. 140, no. Supplement 1, pp. 7382–7383, 2022, doi: 10.1182/blood-2022-160218.

[59] S. Patel, R. C. Ryals, K. K. Weller, M. E. Pennesi, and G. Sahay, “Lipid nanoparticles for delivery of messenger RNA to the back of the eye,” *J. Control. Release*, vol. 303, pp. 91–100, 2019, doi: https://doi.org/10.1016/j.jconrel.2019.04.015.

[60] A. Akinc *et al.*, “The Onpattro story and the clinical translation of nanomedicines containing nucleic acid-based drugs,” *Nat. Nanotechnol.*, vol. 14, no. 12, pp. 1084–1087, 2019, doi: 10.1038/s41565-019-0591-y.

[61] G. Ishii, A. Ochiai, and S. Neri, “Phenotypic and functional heterogeneity of cancer-associated fibroblast within the tumor microenvironment,” *Adv. Drug Deliv. Rev.*, vol. 99, pp. 186–196, 2016, doi: https://doi.org/10.1016/j.addr.2015.07.007.

[62] R. Mhaidly and F. Mechta-Grigoriou, “Fibroblast heterogeneity in tumor micro-environment: Role in immunosuppression and new therapies,” *Semin. Immunol.*, vol. 48, p. 101417, 2020, doi: https://doi.org/10.1016/j.smim.2020.101417.

[63] Y. Xiao, K. Shi, Y. Qu, B. Chu, and Z. Qian, “Engineering Nanoparticles for Targeted Delivery of Nucleic Acid Therapeutics in Tumor,” *Mol. Ther. - Methods Clin. Dev.*, vol. 12, pp. 1–18, 2019, doi: https://doi.org/10.1016/j.omtm.2018.09.002.

[64] M. P. Lokugamage *et al.*, “Optimization of lipid nanoparticles for the delivery of nebulized therapeutic mRNA to the lungs,” *Nat. Biomed. Eng.*, vol. 5, no. 9, pp. 1059–1068, 2021, doi: 10.1038/s41551-021-00786-x.

[65] R. Y. K. Chang and H.-K. Chan, “Lipid nanoparticles for the inhalation of mRNA,” *Nat. Biomed. Eng.*, vol. 5, no. 9, pp. 949–950, 2021, doi: 10.1038/s41551-021-00794-x.

[66] P. Kalyanram, A. Puri, and A. Gupta, “Thermotropic effects of PEGylated lipids on the stability of HPPH-encapsulated lipid nanoparticles (LNP),” *J. Therm. Anal. Calorim.*, vol. 147, no. 11, pp. 6337–6348, 2022, doi: 10.1007/s10973-021-10929-6.

[67] R. C. Ryals, S. Patel, C. Acosta, M. McKinney, M. E. Pennesi, and G. Sahay, “The effects of PEGylation on LNP based mRNA delivery to the eye,” *PLoS One*, vol. 15, no. 10, pp. 1–17, 2020, doi: 10.1371/journal.pone.0241006.

[68] J. A. Kulkarni *et al.*, “Design of lipid nanoparticles for in vitro and in vivo delivery of plasmid DNA,” *Nanomedicine Nanotechnology, Biol. Med.*, vol. 13, no. 4, pp. 1377–1387, 2017, doi: https://doi.org/10.1016/j.nano.2016.12.014.

[69] J. A. Kulkarni, P. R. Cullis, and R. van der Meel, “Lipid Nanoparticles Enabling Gene Therapies: From Concepts to Clinical Utility.,” *Nucleic Acid Ther.*, vol. 28, no. 3, pp. 146–157, Jun. 2018, doi: 10.1089/nat.2018.0721.

[70] F. Sebastiani *et al.*, “Apolipoprotein E Binding Drives Structural and Compositional Rearrangement of mRNA-Containing Lipid Nanoparticles,” *ACS Nano*, vol. 15, no. 4, pp. 6709–6722, Apr. 2021, doi: 10.1021/acsnano.0c10064.

[71] E. Álvarez-Benedicto *et al.*, “Optimization of phospholipid chemistry for improved lipid nanoparticle (LNP) delivery of messenger RNA (mRNA),” *Biomater. Sci.*, vol. 10, no. 2, pp. 549–559, 2022, doi: 10.1039/D1BM01454D.

[72] S. Patel *et al.*, “Naturally-occurring cholesterol analogues in lipid nanoparticles induce polymorphic shape and enhance intracellular delivery of mRNA,” *Nat. Commun.*, vol. 11, no. 1, p. 983, 2020, doi: 10.1038/s41467-020-14527-2.

[73] D. Wang *et al.*, “Antisense microRNA185 loaded liposome for efficient inhibition of the hepatic endogenous microRNA185 level,” *Eur. J. Pharm. Sci.*, vol. 161, p. 105803, 2021, doi: https://doi.org/10.1016/j.ejps.2021.105803.

[74] C. B. Roces *et al.*, “Manufacturing Considerations for the Development of Lipid Nanoparticles Using Microfluidics,” *Pharmaceutics*, vol. 12, no. 11, 2020, doi: 10.3390/pharmaceutics12111095.

[75] C. Webb *et al.*, “Using microfluidics for scalable manufacturing of nanomedicines from bench to GMP: A case study using protein-loaded liposomes,” *Int. J. Pharm.*, vol. 582, p. 119266, 2020, doi: https://doi.org/10.1016/j.ijpharm.2020.119266.

[76] M. Maugeri *et al.*, “Linkage between endosomal escape of LNP-mRNA and loading into EVs for transport to other cells,” *Nat. Commun.*, vol. 10, no. 1, p. 4333, 2019, doi: 10.1038/s41467-019-12275-6.

[77] S. Luozhong *et al.*, “Phosphatidylserine Lipid Nanoparticles Promote Systemic RNA Delivery to Secondary Lymphoid Organs,” *Nano Lett.*, vol. 22, no. 20, pp. 8304–8311, Oct. 2022, doi: 10.1021/acs.nanolett.2c03234.

[78] M. J. Munson *et al.*, “A high-throughput Galectin-9 imaging assay for quantifying nanoparticle uptake, endosomal escape and functional RNA delivery,” *Commun. Biol.*, vol. 4, no. 1, p. 211, 2021, doi: 10.1038/s42003-021-01728-8.

[79] S. L. Yefimova, G. Y. Gural’chuk, A. V Sorokin, Y. V Malyukin, I. A. Borovoy, and A. S. Lubyanaya, “Hydrophobicity effect on interactions between organic molecules in nanocages of surfactant micelle,” *J. Appl. Spectrosc.*, vol. 75, no. 5, pp. 658–663, 2008, doi: 10.1007/s10812-008-9108-4.

[80] M. D. Ludes and M. J. Wirth, “Single-Molecule Resolution and Fluorescence Imaging of Mixed-Mode Sorption of a Dye at the Interface of C18 and Acetonitrile/Water,” *Anal. Chem.*, vol. 74, no. 2, pp. 386–393, Jan. 2002, doi: 10.1021/ac010943u.

[81] K. Shimizu, A. A. de Freitas, and C. M. Burba, “Cation-Anion and Cation-Cation Interactions in Mixtures of Hydroxy-functionalized and Aprotic Ionic Liquids,” *J. Ion. Liq.*, vol. 2, no. 1, p. 100022, 2022, doi: https://doi.org/10.1016/j.jil.2022.100022.

[82] C. Cheng, O. Trzcinski, and L. C. Doering, “Fluorescent labeling of dendritic spines in cell cultures with the carbocyanine dye ‘DiI’.,” *Front. Neuroanat.*, vol. 8, p. 30, 2014, doi: 10.3389/fnana.2014.00030.

[83] D. Vela and L. Maximilian Buja, “Chapter 2 - Pathological Assessment of Experimental Models of Stem Cell and Other Regenerative Therapies,” E. C. Perin, L. W. Miller, D. A. Taylor, and J. T. B. T.-S. C. and G. T. for C. D. Willerson, Eds. Boston: Academic Press, 2016, pp. 13–23.

[84] T. Zeuthen and N. MacAulay, “Transport of water against its concentration gradient: fact or fiction?,” *Wiley Interdiscip. Rev. Membr. Transp. Signal.*, vol. 1, no. 4, pp. 373–381, 2012, doi: https://doi.org/10.1002/wmts.54.

[85] C. W. Scales, A. J. Convertine, and C. L. McCormick, “Fluorescent Labeling of RAFT-Generated Poly(N-isopropylacrylamide) via a Facile Maleimide−Thiol Coupling Reaction,” *Biomacromolecules*, vol. 7, no. 5, pp. 1389–1392, May 2006, doi: 10.1021/bm060192b.

[86] C. C. Visser *et al.*, “Coupling of Metal Containing Homing Devices to Liposomes via a Maleimide Linker: Use of TCEP to Stabilize Thiol-groups without Scavenging Metals,” *J. Drug Target.*, vol. 12, no. 9–10, pp. 569–573, 2004, doi: 10.1080/10611860400010689.

[87] M. Nurmik, P. Ullmann, F. Rodriguez, S. Haan, and E. Letellier, “In search of definitions: Cancer-associated fibroblasts and their markers,” *Int. J. Cancer*, vol. 146, no. 4, pp. 895–905, 2020, doi: https://doi.org/10.1002/ijc.32193.

[88] A. Arina *et al.*, “Tumor-associated fibroblasts predominantly come from local and not circulating

precursors," *Proc. Natl. Acad. Sci.*, vol. 113, no. 27, pp. 7551–7556, 2016, doi: 10.1073/pnas.1600363113.

[89] R. Tanaka *et al.*, "Interleukin-8 produced from cancer-associated fibroblasts suppresses proliferation of the OCUCh-LM1 cancer cell line," *BMC Cancer*, vol. 22, no. 1, p. 748, 2022, doi: 10.1186/s12885-022-09847-z.

[90] M. Sha *et al.*, "Isolation of cancer-associated fibroblasts and its promotion to the progression of intrahepatic cholangiocarcinoma," *Cancer Med.*, vol. 7, no. 9, pp. 4665–4677, 2018, doi: https://doi.org/10.1002/cam4.1704.

[91] S. Y. Ha, S.-Y. Yeo, Y. Xuan, and S.-H. Kim, "The Prognostic Significance of Cancer-Associated Fibroblasts in Esophageal Squamous Cell Carcinoma," *PLoS One*, vol. 9, no. 6, pp. 1–9, 2014, doi: 10.1371/journal.pone.0099955.

[92] G.-M. Zhang, Z.-W. He, Y. Li, and J.-J. Li, "Gene silencing of Col1α1 by RNAi in rat myocardium fibroblasts," vol. 44, no. 6, pp. 803–809, 2019, doi: doi:10.1515/tjb-2018-0493.

[93] R. Ando, A. Sakai, T. Iida, K. Kataoka, Y. Mizutani, and A. Enomoto, "Good and Bad Stroma in Pancreatic Cancer: Relevance of Functional States of Cancer-Associated Fibroblasts," *Cancers (Basel).*, vol. 14, no. 14, 2022, doi: 10.3390/cancers14143315.

[94] T. J. Harryvan *et al.*, "Gastrointestinal cancer-associated fibroblasts expressing Junctional Adhesion Molecule-A are amenable to infection by oncolytic reovirus," *Cancer Gene Ther.*, 2022, doi: 10.1038/s41417-022-00507-9.

[95] G. Gstraunthaler, T. Lindl, and J. van der Valk, "A plea to reduce or replace fetal bovine serum in cell culture media.," *Cytotechnology*, vol. 65, no. 5, pp. 791–793, Oct. 2013, doi: 10.1007/s10616-013-9633-8.

[96] A. Algarni, E. H. Pilkington, E. J. A. Suys, H. Al-Wassiti, C. W. Pouton, and N. P. Truong, "In vivo delivery of plasmid DNA by lipid nanoparticles: the influence of ionizable cationic lipids on organ-selective gene expression," *Biomater. Sci.*, vol. 10, no. 11, pp. 2940–2952, 2022, doi: 10.1039/D2BM00168C.

8. Appendix

Gene	Forward Primer	Reverse Primer
αSMA	GACAGCTACGTGGGTGACGAA	TTTTCCATGTCGTCCCAGTTG
COL1A1	GTACTGGATTGACCCCAACC	CGCCATACTCGAACTGGAAT
PDGFRB	AGGCAAGCTGGTCAAGATCT	GCTGTTGAAGATGCTCTCCG
ITGA5	CAACTTCTCCTTGGACCCCC	GTCCTCTATCCGGCTCTTGC

Table A 1.Primers used in qPCR

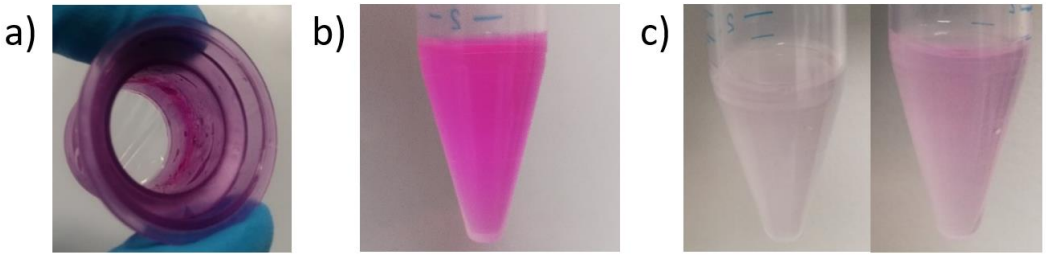

Figure A 1. Dil loss during the LNP fabrication process for "20ml/min" and "1:5 ratio" LNPs. B) Before dialysis LNPs formulations had distinct intense pink color. However after the dialysis c) loss of the dye was noticed. a) Dialysis filter with the pink residue.

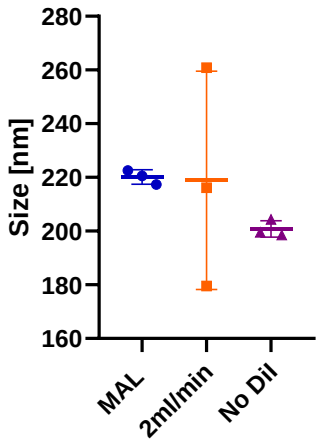

Figure A 2. Size reproducibility of LNP formulation.

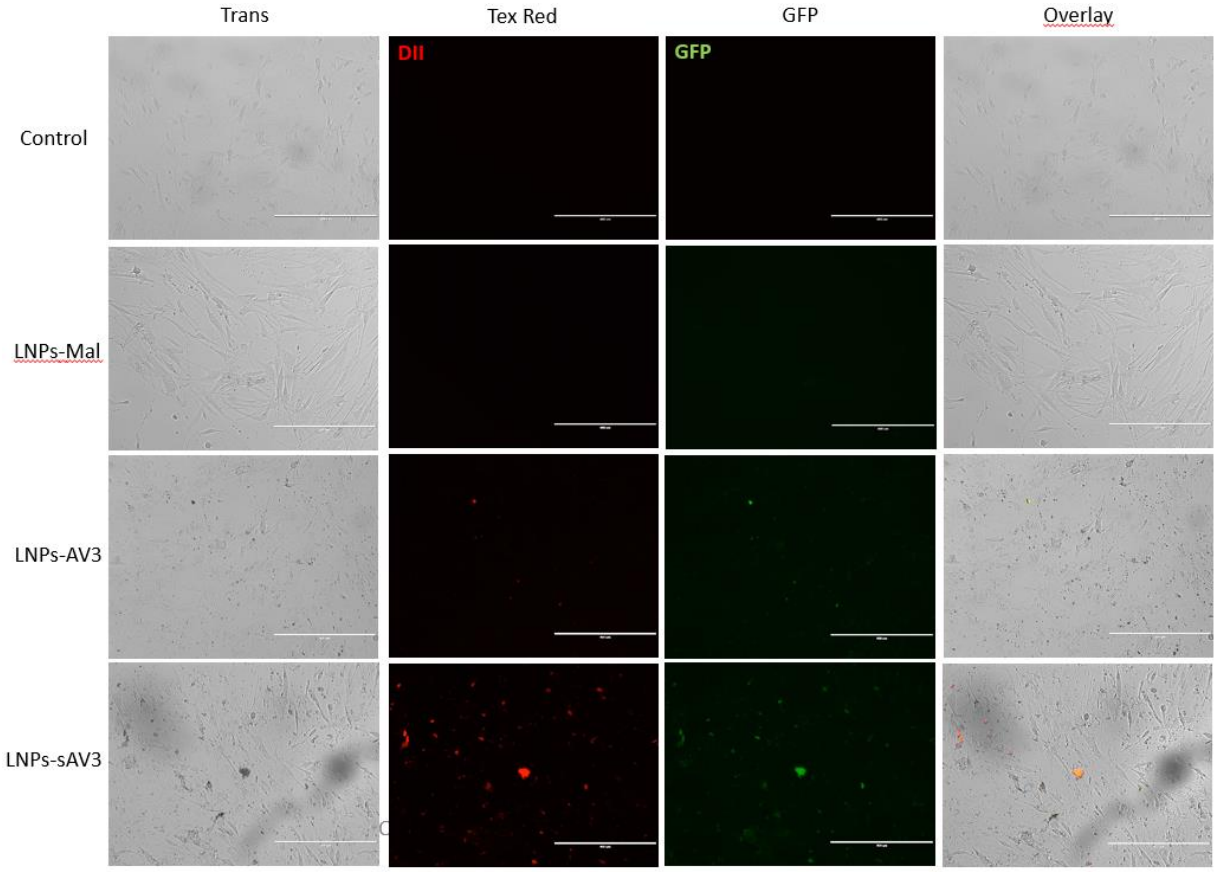

Figure A 3. Representative microsocpy images of quiescent PSCs tarnsfection with LNPs-MAL, LNPs-AV3 or LNPs-sAV3 containing a mix of total RNA RAW-eGFP positive cells and eGFP mRNA (3:1) and DiI dye for 24h. The side headlines indicate the transfection conditions. For wach condition the first picture displays just cells, the second one represetd just red DiI signal, the third picture reprsents mRNA eGFP signal and the fourth picture reprsents an overalsy of the three previous pictures. The uptake study was performed using LNPs-MAL, LNPs-AV3 or LNPs-sAV3 in the amount that corresponds to 100 ng of total RNA RAW-eGFP positive cells and eGFP mRNA.

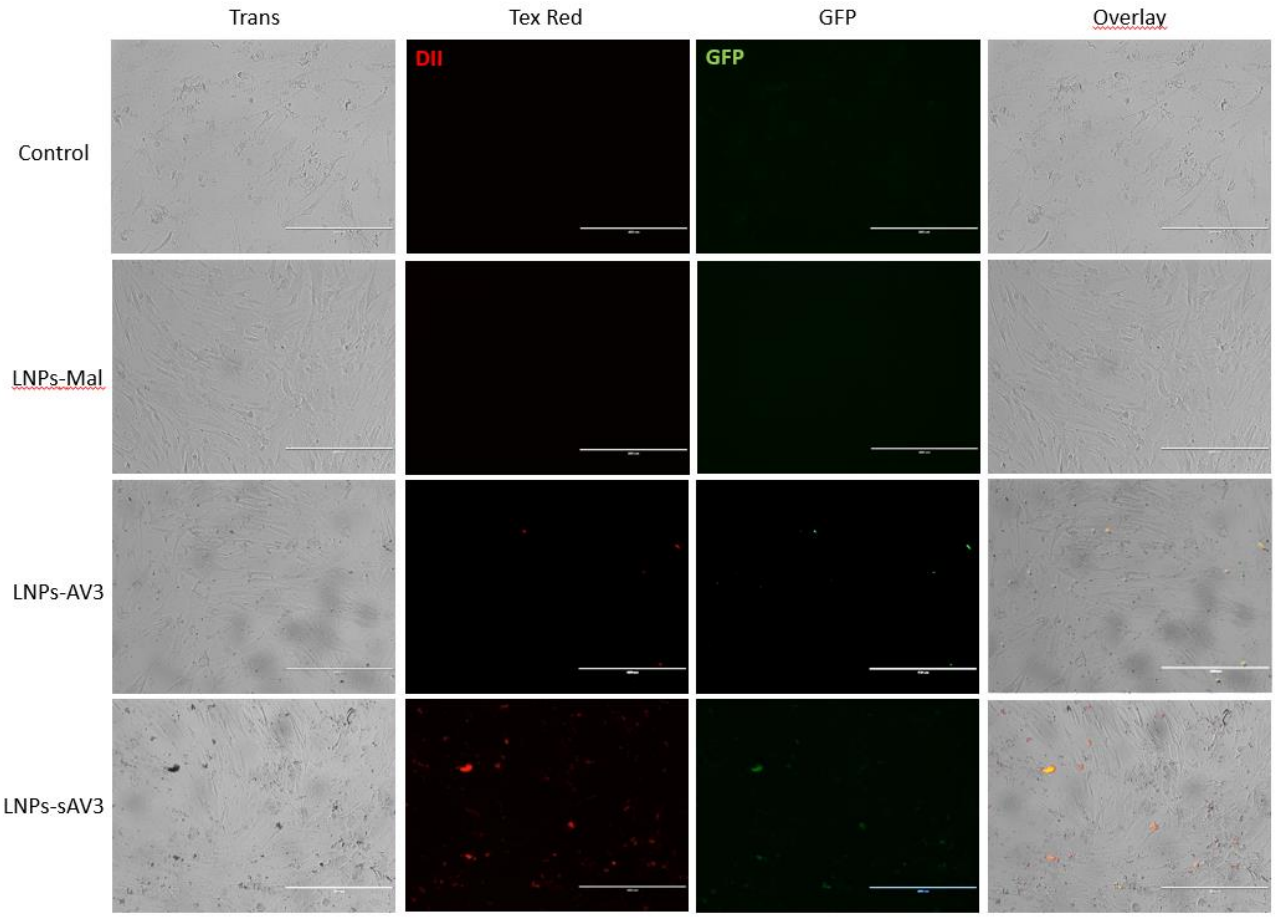

Figure A 4. Representative microsocpy images ofactivated PSCs tarnsfection with LNPs-MAL, LNPs-AV3 or LNPs-sAV3 containing a mix of total RNA RAW-eGFP positive cells and eGFP mRNA (3:1) and DiI dye for 24h. The side headlines indicate the transfection conditions. For wach condition the first picture displays just cells, the second one represetd just red DiI signal, the third picture reprsents mRNA eGFP signal and the fourth picture reprsents an overalsy of the three previous pictures. The uptake study was performed using LNPs-MAL, LNPs-AV3 or LNPs-sAV3 in the amount that corresponds to 100 ng of total RNA RAW-eGFP positive cells and eGFP mRNA.

9. List of Figures

10. List of Tables